Pontificia Universidad Católica del Perú

Escuela de Posgrado

Investigation of the rheological behavior of polyborosiloxane

Tesis para obtener el grado académico de Maestro en Ingeniería y Ciencia de los Materiales que presenta:

Dante Aaron Ramirez Mestanza

Asesor PUCP (PUCP):   *Rolf Grieseler*
Co-Asesor de la Universidad no PUCP: *Lena Zentner*

Lima, 2024

Informe de Similitud

Yo, Rolf Grieseler, docente de la Escuela de Posgrado de la Pontificia Universidad Católica del Perú, asesor de la tesis titulada **"Investigation of the rheological behavior of polyborosiloxane"**, del autor Dante Aaron Ramirez Mestanza, código PUCP: 20134740, alumno de la Maestría en Ingeniería y Ciencia de los Materiales, dejo constancia de lo siguiente:

- El mencionado documento tiene un índice de puntuación de similitud de 17%. Así lo consigna el reporte de similitud emitido por el software *Turnitin* el 18/01/2024.
- He revisado con detalle dicho reporte y la Tesis o Trabajo de Suficiencia Profesional, y no se advierte indicios de plagio.
- Las citas a otros autores y sus respectivas referencias cumplen con las pautas académicas.

Lima, 18 de enero de 2024.

Grieseler, Rolf	
CE: 001660902	Firma
ORCID: 0000-0001-5307-7755	
	R. Grieseler

Resumen

Polyborosiloxano, una silicona derivada de la modificación del polidimetilsiloxano con grupos $B(OH)_x$ en sus cadenas poliméricas, exhibe propiedades únicas, como su comportamiento reológico y capacidad de autorregeneración. Estas características se explican a través de su estructura química: ante deformaciones lentas, los enlaces se rompen y regeneran secuencialmente, permitiendo el movimiento de las cadenas. No obstante, al superar un límite, estos enlaces actúan como puntos de reticulación, aumentando la rigidez del material. Aunque se ha investigado la relación entre la estructura química y las propiedades, la influencia de los métodos de síntesis y diversos estímulos aún no se ha explorado completamente.

En esta investigación, se fabricaron muestras de polyborosiloxano utilizando polidimetilsiloxanos con diferentes viscosidades. Estas muestras se clasifican en tres categorías: la primera consiste en polyborosiloxanos puros, la segunda en muestras obtenidas mezclando dos precursores de viscosidades diferentes en proporciones en peso (20/80, 40/60, 60/40 y 80/20 %), y la tercera en mezclas de los polyborosiloxanos puros siguiendo las mismas proporciones que la segunda categoría.

Se realizaron pruebas de barrido de amplitud y frecuencia para evaluar las propiedades reológicas de las muestras. Además, se emplearon diversas técnicas para caracterizar la estructura química y morfología, con el fin de identificar los diferentes enlaces químicos y residuos de ácido bórico no reaccionado. Con el propósito de analizar el impacto de las vibraciones, se realizó una prueba de cambio de forma a diversas frecuencias para determinar las tasas de deformación de las muestras de polyborosiloxano puro.

El análisis químico y morfológico de las muestras confirma la existencia de enlaces Si-O-B en la estructura, validando la correcta síntesis del polyborosiloxano. Además, se identificaron residuos de ácido bórico no reaccionado en todas las muestras sometidas a ensayo. En relación con la caracterización reológica, se constató que las muestras pertenecientes a la segunda categoría exhibieron una distribución más homogénea en la influencia de uno de los polyborosiloxanos en sus propiedades en comparación con las de la tercera categoría. Además, en estas últimas, la adición de polyborosiloxano de menor viscosidad afectó el comportamiento reológico para valores superiores al 40%. Los gráficos de cambio de forma evidencian el impacto de los estímulos mecánicos en la capacidad de retención de forma del polyborosiloxano. En el caso de la muestra de menor viscosidad, se registraron las mayores y menores deformaciones a $0\,Hz$ y $1\,Hz$, respectivamente; en contraste, para la otra muestra, dichas frecuencias fueron de $5\,Hz$ y $1\,Hz$.

Abstract

Polyborosiloxane, also known as Shear Stiffening Gel, is a silicon-based elastomer resulting from the modification of polydimethylsiloxane with $B(OH)_x$ groups. This material possesses exceptional properties, including unique viscoelasticity and self-healing ability. Its chemical structure explains two entirely reversible mechanical behaviors: at low stress rates, polyborosiloxane exhibits a viscous fluid behavior due to the relaxation of dynamic bonds, and at high stress rates, its behavior transitions from viscous to rubbery as a result of the locking of these dynamic bonds. Previous investigations have explored the relationship between the chemical structure and its properties. However, there is insufficient information regarding the influence of synthesis methods and different stimuli (vibrations or magnetic field) for its application in soft robotics.

In this thesis, various polyborosiloxane samples were created using polydimethylsiloxanes with two different viscosities, one being higher than the other. These samples are divided into three categories. The first category consists of pure polyborosiloxanes synthesized with the mentioned polydimethylsiloxane precursors. The second category involves synthesized samples by mixing the two polydimethylsiloxane precursors in different weight ratios (20/80, 40/60, 60/40, and 80/20). The third group includes samples formed by mixing the two pure polyborosiloxanes of the first category in the same ratios as the second group.

The rheological properties of these samples are evaluated through amplitude and frequency sweep tests. Additionally, various techniques are employed to characterize the chemical structure and morphology, revealing the diverse bonds present in the samples. To explore the impact of vibrations on polyborosiloxane properties, a shape change test is conducted at various vibration frequencies to identify the frequencies at which a semi-spherical polyborosiloxane sample exhibits the lowest and highest deformation rates under its own weight in a gravitational field.

The characterization results reveal the presence of characteristic chemical bonds Si-O-B in the structure of the synthesized polyborosiloxane samples, along with traces of unreacted boric acid. The analysis based on rheological testing leads to the conclusion that the samples from the second category, involving the mixing of polydimethylsiloxane precursors, display a more homogeneous distribution compared to those in the third category. Moreover, in the samples of the third category, the addition of polyborosiloxane synthesized with the lower viscosity precursor starts to influence on the rheological behavior for values over 40 % of this material. The shape change graphics demonstrate the impact of mechanical stimuli on the shape-retainability of polyborosiloxane. Therefore, for the polyborosiloxane sample made with the lower viscosity precursor, the highest and lowest deformations were observed at 0 Hz and 1 Hz, respectively. In contrast, for the other sample, these frequencies were recorded at 5 Hz and 1 Hz.

Contents

List of Figures

List of Tables

Acronyms Glossary

This section presents a list of acronyms and their corresponding meanings utilized in this thesis.

ATR   Attenuated Total Reflectance

BA   Boric Acid

BP   Bouncing Putty

CI   Carbonyl Iron

DCDMS   Dichlorodimethylsilane

FTIR   Fourier Transform Infrared Spectroscopy

IoT   Internet Of Things

IVC   Inferior Vena Cava

LDH   Layered Double Hydroxide

LVER   Linear Viscoelastic Region

MR   Magneto-Rheological Fluids

PBS   Polyborosiloxane

PDMS   Polydimethylsiloxane

SEM   Scanning Electron Microscopy

SMAs   Shape Memory Alloys

SMs   Smart Materials

SP   Silly Putty

SSG   Shear Stiffening Gel

TGA   Thermal Gravimetric Analysis

List of Symbols

Symbol	Definition	Units
G'	Storage modulus	Pa
G''	Loss modulus	Pa
$G*$	Complex modulus	Pa
v	Velocity	$\frac{\mathrm{m}}{\mathrm{s}}$
η	Viscosity	Pa s
τ	Shear stress	Pa
$\dot{\gamma}$	Shear stress rate	Pa s
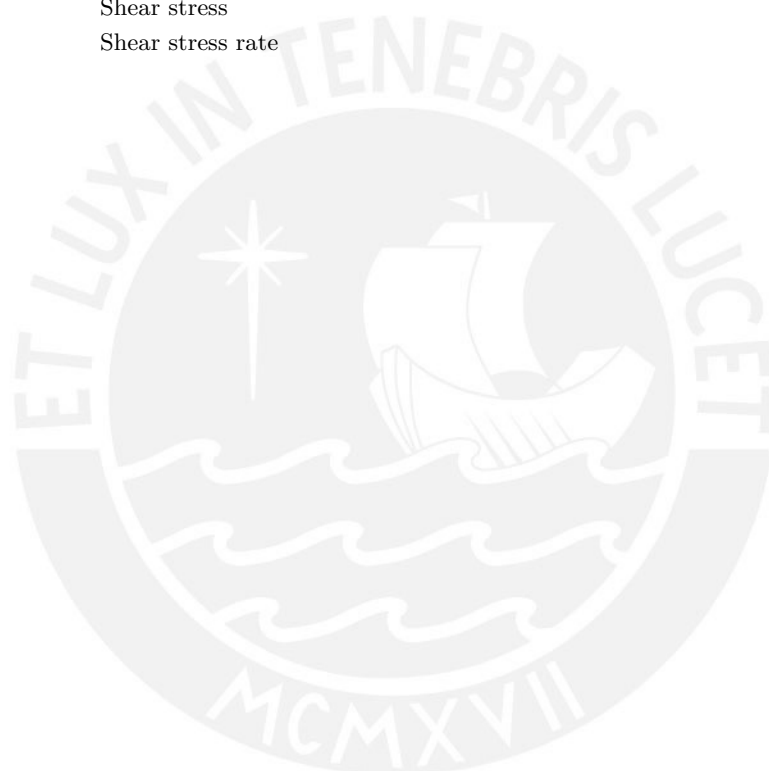
1. Introduction

Smart Materials (SMs) are an interesting field of materials due to the possibility of modifying their properties under the influence of different stimuli: heat, magnetic field, electric field, or mechanical stresses. This material has been applied successfully in various applications such as biomedical, aerospace, soft robotics, and compliant systems. Modifying its properties enables different possibilities to obtain precise control with less energy usage in these systems. An example of this smart material is Polyborosiloxane (PBS), known by various names like Shear Shear Stiffening Gel (SSG), Bouncing Putty (BP), or Silly Putty (SP). These material exhibit exceptional characteristics, including unique viscoelasticity, self-healing ability, ease of synthesis, and the possibility of adding different fillers to modify its behavior under a specific stimulus. [32]

Polyborosiloxane is a silicon-based elastomer consisting of $B(OH)_x$ (where x can be two, one, or zero depending on the mixing ratio during the synthesizing process) group modification of Polydimethylsiloxane (PDMS) chains. Different precursors can fabricate this elastomer, but the most investigated and easy to process are the PDMS and Boric Acid (BA) via condensation reaction. [18]

The PBS has two different mechanical behaviors that are completely reversible, and it can be explained by its chemical structure. When a slow stress rate is applied, the dynamic bonds in the structure break over time allowing chain movement and enabling a viscous fluid behavior. However, if this stress rate exceeds a critical value, these bonds act as crosslinking points changing the behavior of PBS from viscous to rubbery. [15]

Some investigations aimed to find a relation between the chemical structure and properties of PBS. They modified this structure varying the parameters and precursors of PBS synthesis process. An example of this is the research of Kurkin et al. [18], where the objective was to study the influence of the viscosity of the PDMS precursor on the number of sticker groups and PBS properties. Figure 1.1 shows a schematic illustration of two PBS structures based on the literature and the results of Kurkin et al.: The PBS25 made with a PDMS that has a viscosity of $25 \cdot 10^{-6} \frac{m^2}{s}$ and the PBS18000 made with a PDMS that has a viscosity of $18 \cdot 10^{-3} \frac{m^2}{s}$. This scheme shows that the density of supramolecular interactions decreases with a higher molecular weight (viscosity) of the PDMS due to the fewer boron modifications in the chain ends. In addition, Seerapan et al. [41] investigated the influence of molecular weight of the PDMS on unimodal and bimodal network of the PBS and its viscoelasticity. They found that the PDMS with the shortest viscosity ($90\text{-}150 \cdot 10^{-6} \frac{m^2}{s}$) presents the highest relaxation time of $1.59\,s$ and the best fit to the Maxwell model. These investigations show the importance of molecular weight in the rheological behavior of PBS.
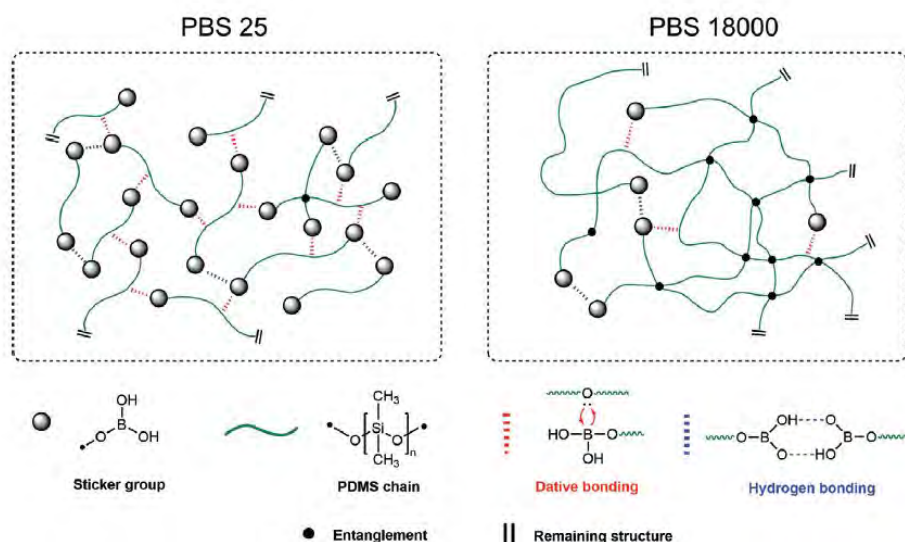
Figure 1.1.: Schematic illustration of molecular structures and interactions of PBS 25 and PBS 18 000 [18]

The mentioned investigations provide fundamental information about the influence of molecular weight and synthesis parameters in the properties of PBS. However, they studied this relation using a single precursor for each PBS and not mixing two or more precursors before the synthesis or mixing different PBS. Therefore, they evaluate this material in normal conditions without an stimulus such as magnetic field or vibrations, which are required to apply smart materials in soft robotics.

In this investigation, the main objective is to find the influence of diverse mixing ratios of two PDMS precursors with different viscosity in the rheological properties of the PBS and the effect of mechanical stimuli on the behavior. For this purpose, the master thesis focuses on the following aspects:

- literature review on the current state of the art of polyborosiloxane and its common behavior descriptions;

- defining the experimental procedure to determine the dynamic mechanical properties of PBS and investigating its responses under different stimuli;

- fabricating PBS samples using two types of polydimethylsiloxanes and boric acid with different mixing methods and five mixing ratios;

- chemical and morphological characterization of PBS samples through techniques such as Fourier Transform Infrared Spectroscopy (FTIR), Raman spectroscopy, Scanning Electron Microscopy (SEM), and stereoscopy;

- rheological characterization of PBS samples through amplitude and frequency sweep tests;

- shape change characterization of PBS samples by different mechanical stimuli.

2. Theoretical Fundamentals

First, this chapter provides a brief background on smart materials and their various applications. Then, it outlines various methods for synthesizing polyborosiloxane, explores the possible chemical structures of this material, and discusses its correlation with mechanical properties. Subsequently, it offers a concise background on rheology, emphasizing diverse flow behaviors of polymers, viscoelastic properties, and mathematical models capable of describing viscoelasticity.

2.1. Smart Materials

A long time ago, materials used to be classified into three main categories: polymers, ceramics, and metals. These are commonly referred to as standard materials and have been widely utilized in various fields, including civil engineering, machinery, transportation, and others. However, in recent decades, advancements in science and technology have resulted in the synthesis of new materials, introducing a new category: smart materials. [3]

Smart materials are substances with the capability to modify their behavior and properties in response to various stimuli or environmental conditions. This unique ability has facilitated their application in numerous technological developments, contributing to the enhancement of people's health and overall quality of life. An illustrative example is the evolution of robotics, transitioning from rigid-bodied constructions to soft robots utilizing compliant systems and smart materials. With these innovative materials, soft robots can potentially regenerate and adapt themselves to diverse situations. [63]

Smart materials are categorized according to their properties, which can be passive or active, or based on the external stimuli to which they can react. Following paragraphs explain a few of these classifications.

2.1.1. Shape Memory Alloys

Shape Memory Alloys (SMAs) are materials with a unique characteristic: the ability to restore their initial shape after deformation through a stimulus of temperature. This effect occurs due to the transformation from the crystalline phase of martensite to austenite caused by external energy. At ambient temperature, these alloys exhibit a martensite structure, which can be easily deformed. After this deformation, the alloy is heated, causing a phase change from martensite to austenite, thereby returning to its original shape. One of the most well-known SMAs is

Nitinol, an alloy of nickel and titanium in approximately equal proportions (see Figure 2.1). [43], [50]
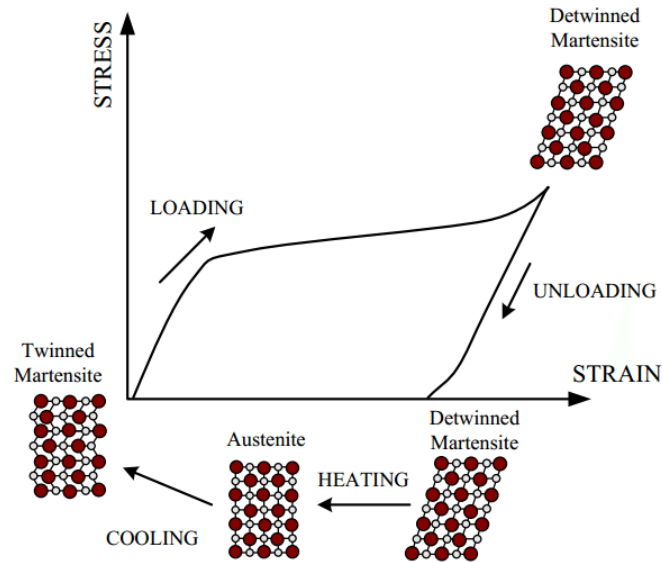
Figure 2.1.: Shape memory effect [51]

The diverse applications of SMAs extend across healthcare, aerospace, automotive, and Internet Of Things (IoT). In the healthcare sector, for instance, SMAs have found application in surgical filtration devices due to their high deformation capacity, extended fatigue life, wear resistance, and shape memory effect. Utilizing Nitinol as the base material, Inferior Vena Cava (IVC) filters have minimized the invasiveness of the required surgery for its insertion. The initial Nitinol IVC filter was developed by C.R. Bard and named as Simon filter (see Figure 2.2). This device was utilized in the treatment of pulmonary embolism. The filter comprises two main components: the upper section, equipped with a filter mesh to capture blood clots, and the lower section, consisting of six Nitinol expandable struts that arc as the anchoring basal component. [61]
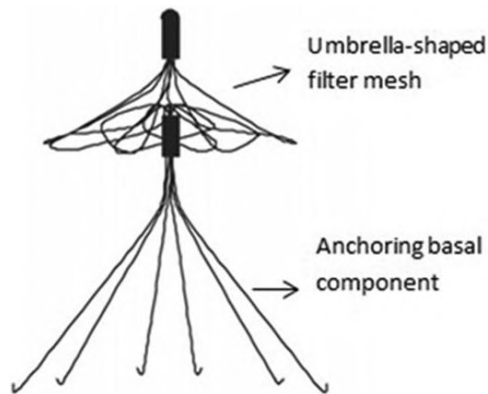
Figure 2.2.: Scheme of a IVC Simon Filter [61]

2.1.2. Piezoelectric Materials

Piezoelectric materials can be either inorganic or organic substances with the ability to transform electricity into mechanical force and vice versa. This characteristic allows to use them for energy harvesting from various sources, minimally invasive sensors, drug delivery systems, and storage systems, shown in Figure 2.3. [65] There is a variety of piezoelectric materials, selected based on their applications. For energy harvesting, nanostructured materials, piezoelectric polymers, and piezoelectric polymer nanocomposites are preferred. [22]
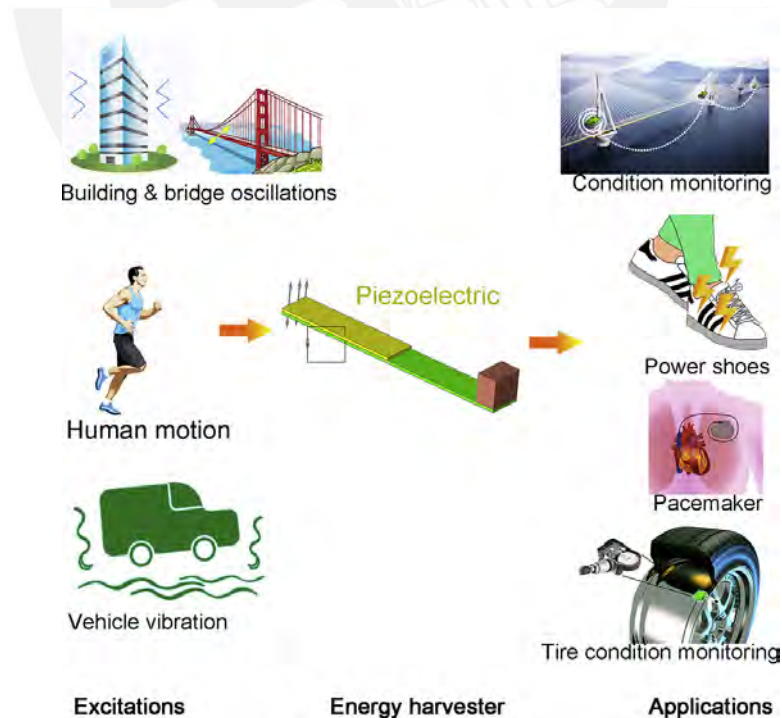
Figure 2.3.: Applications of piezoelectric materials in different areas [62]

In 2018, Nabavi et al. [24] conducted an investigation on a piezoelectric device designed to convert the energy of ocean waves into electrical energy. Initially, they derived the electromechanical equations of motion for the energy equations and validated them. Subsequently, they examined the installed systems in offshore buoys, determining that the generated energy was sufficient to sustain the electrical devices on the buoys. The prototype of this device is shown in Figure 2.4.
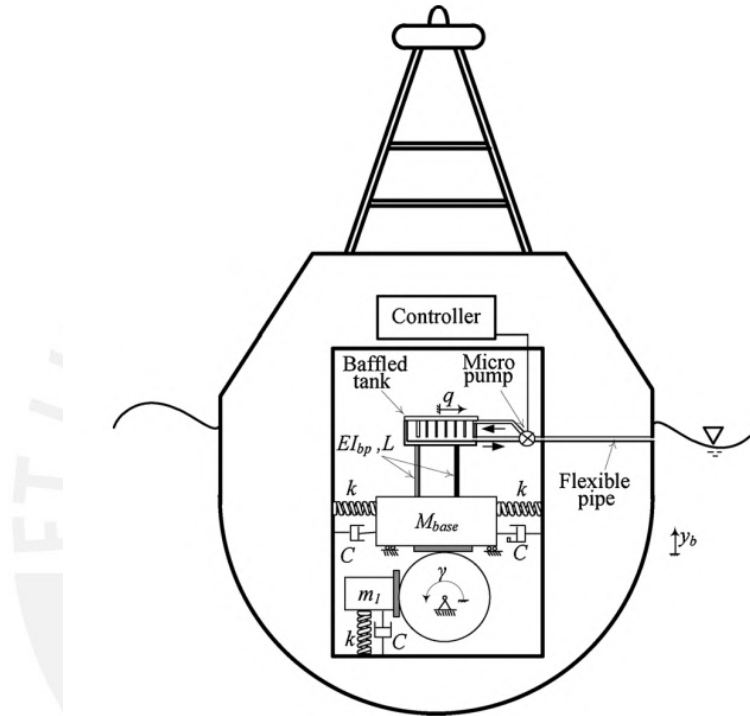
Figure 2.4.: Scheme of the investigated self tuning buoy [24]

2.1.3. Magneto-Rheological Materials

Magneto-Rheological Fluids (MR) belong to a class of materials capable of modifying their rheological behavior under the influence of a magnetic field. These materials are created by adding nanometer- or micrometer-sized ferromagnetic fillers to the matrix. The interest in this material arises from its ability to rapidly alter its properties by changing the external magnetic field. However, a challenge in their application derive from the sedimentation of MR due to differences in viscosity between the fillers and the matrix. To overcome this issue, some researchers have reduced the particle size to sub-micron or nanometer dimensions, enhancing the stability of the composite. [60]

In 2016, Wang et al. [57] incorporated Carbonyl Iron (CI) into polyborosiloxane samples to investigate the impact of their percentage on mechanical and rheological properties. The

samples were prepared with CI concentrations of 15 %, 30 %, 45 %, 60 %, and 75 %, and were tested at various magnetic field intensities: 0, 100, 200, and 300 mT. The results revealed that the shear stiffening performance of these composites was stable with a maximum yield strain of 17.2 %, which is associated with phase transitions from a viscous-liquid state to an elastomeric state and eventually to a glassy state under impact. The progression of these states is linked to the strain rate and is illustrated in Figure 2.5.
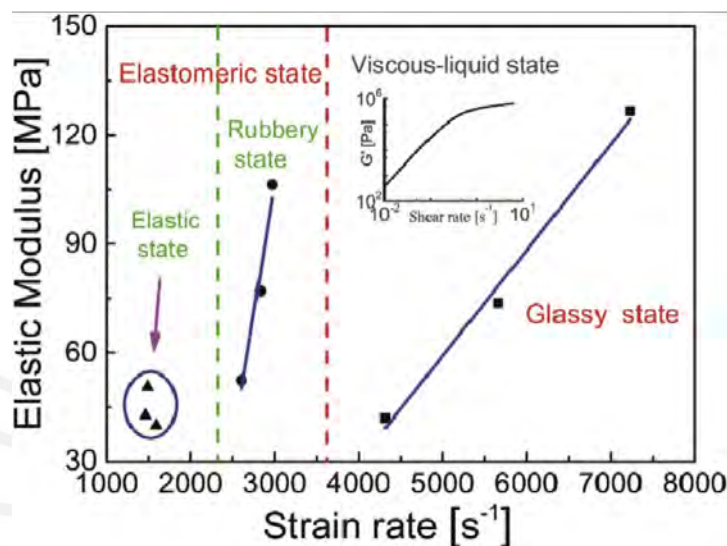
Figure 2.5.: Phase transitions with the change of elastic modulus for 45% of CI at different strain rates [57]

2.2. Polyborosiloxane

Polyborosiloxane is important as a smart material due to its capacity to change its rheological properties under different stimuli, self-healing ability, and the possibility of fabricating a wide variety of composites. These properties depend on the molecular structure of PBS, which is influenced by the molecular mass of the PDMS precursor. Some applications of this material are in sensors, e-skins, anti-impact devices, dampers, and others. [49]

2.2.1. Chemical structure of Polyborosiloxane

In the chemical structure of the PBS, the main end group is the $Si-O-B(OH)_2$, which is responsible for the rheological behavior of this material due to the boron-oxygen dynamic covalent bonds (Si-O:B) and hydrogen bonds. These bonds, at low-stress rates, allow sufficient time for relaxation and reconnection, facilitating the chain movement of PBS and causing it to act as a viscous fluid. However, when the stress exceeds a critical value, these bonds act as crosslinked points, changing the material's behavior from viscous to elastic as a rubber (see Figure 2.6). Furthermore, certain B-O-B functional groups can be present in the polymer

chains of PBS. This presence means a partial condensation reaction between BA molecules due to the random scission effect or sedimentation during the process. [18], [66]
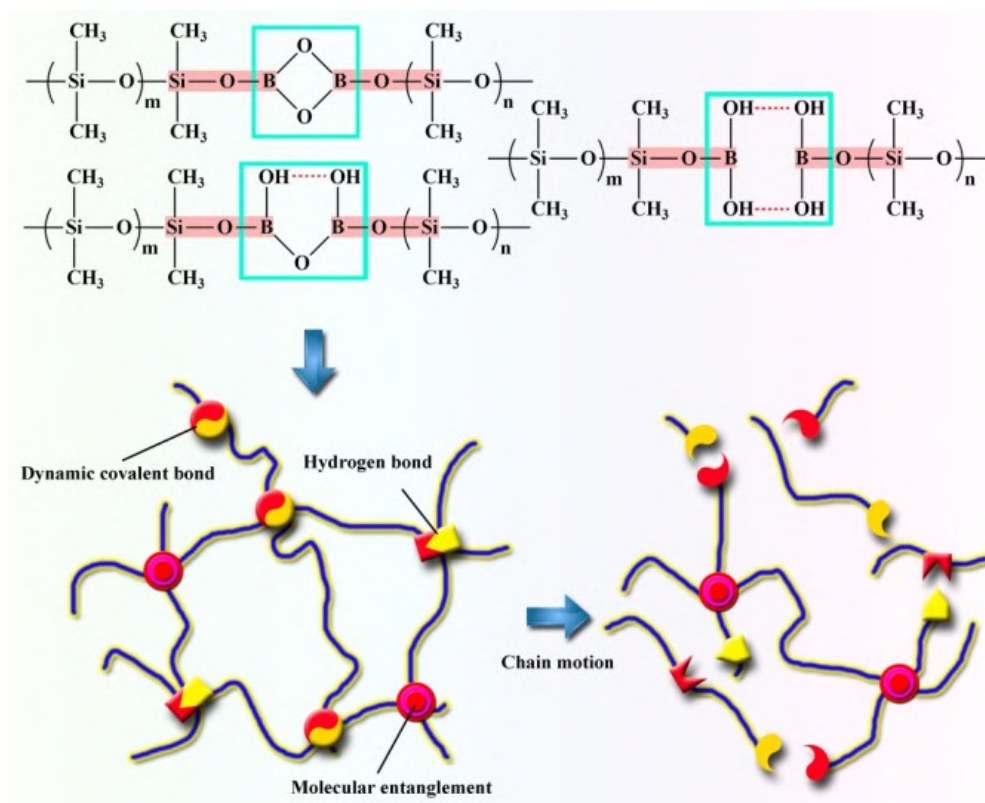
Figure 2.6.: Representation of the PBS chemical structure and its supra-molecular interactions [66]

Regarding the synthesis process of PBS using BA and PDMS as precursors, three possible chemical structures have been widely investigated (see Figure 2.7). Structure I has oxygen dynamic bonds (Si-O: B) and hydrogen bonds, which are associated with the direct condensation reaction between both precursors. In Structure II, B-O-B moieties are observed, which indicates polymerization between BA molecules. Structure III results from the formation of cyclic PBS molecules due to an additional reaction of boron molecules. The probability of obtaining these three structures depends on the interaction between the available OH groups of the PDMS and the boron atoms of BA. Therefore, it is possible to control the final structure of the PBS by adjusting the mixing ratio of PDMS/BA or using different PDMS precursors. [18]
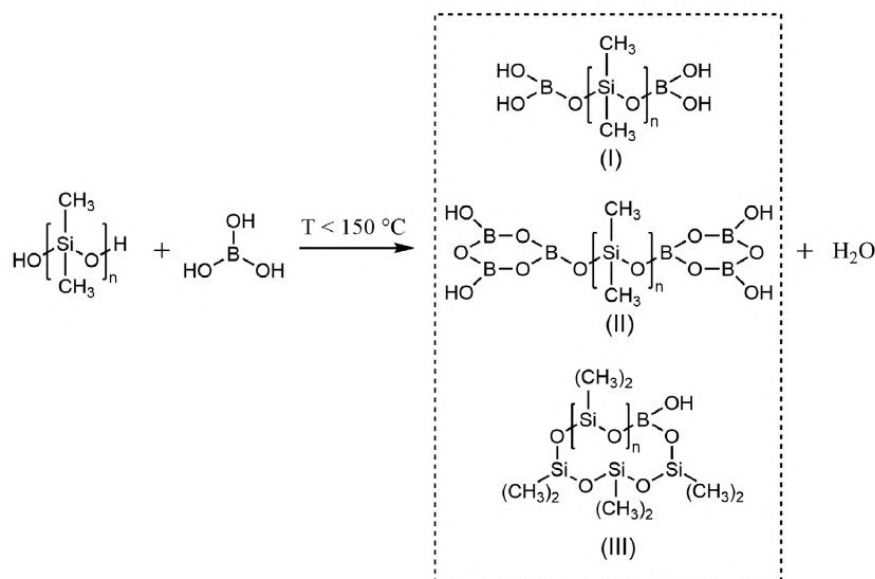
Figure 2.7.: Possible chemical configurations of PBS: (a) structure type I; (b) structure type II; (c) structure type III [18]

2.2.2. Methods of synthesis of Polyborosiloxane

As explained before, the PBS is a PDMS derivative with $B(OH)_x$ groups, that behave as sticker-like bonds and enable this material's unique viscoelasticity. This material's basic synthesis process consists of a PDMS and BA condensation reaction at different temperatures. However, it has disadvantages due to the possibility of reaction between BA molecules, random scission of PDMS chains, or unreacted BA moieties. Zinchenko et al. [68] studied the reaction of these precursors at temperatures below and above $150\,°C$ using Fourier Transform Infrared Spectroscopy (FTIR). The test results showed that above this temperature, the PBS presents B-O-B bonds, which correspond to the BA reaction due to the random chain scission of PDMS. [67]

For this reason, some researchers preferred to synthesize PBS at temperatures below $150\,°C$ to obtain a viscoelastic material. For example, Tang et al. [49] studied a synthesis of structure-controlled polyborosiloxane using PDMS with different molecular masses. In this investigation, they selected a temperature of $120\,°C$, but they added a solvent toluene to reduce the viscosity of the mix, particularly for the PDMS precursors with high molecular masses.

On the other hand, some researchers designed synthetic procedures using different precursors to obtain PBS at lower temperatures than the synthesized process with PDMS and BA. Vale et al. [55] fabricated PBS using Dichlorodimethylsilane (DCDMS) and BA at $90\,°C$ by using two different methods: condensation polymerization and solution polymerization with Layered Double Hydroxide (LDH) as solvent and solid carbon dioxide as external coolant. The results showed that the fabricated material behaved as the bouncing putty with remarkable

viscoelasticity of 80 %. rebound due to the terminal hydroxyl groups present in the chemical structure. Nevertheless, the samples with an excess of DCDMS presented a viscous liquid behavior due to the lack of hydroxyl groups. Another investigation synthesized PBS without Si-O-B bonds, incorporating derivatives of substituted boric acid to enhance its stability under external factors such as atmospheric moisture. This material exhibited properties similar to the original, thus still classified as PBS. The primary functional group of this modified silicone is the Si-Ar-B(OH)$_2$. [8]

2.2.3. Applications of Polyborosiloxane

The first PBS was synthesized in the 1950s, and it has been applied in different areas due to its unusual properties, such as its viscoelasticity, self-healing capacity, high thermal stability, and molecular interactions with organic or inorganic moieties. For example, this material was used to obtain a LDH-based and silicon-PBS coating that showed a thermal stability of 700 °C with low mass losses and flame-retardant properties. Another application of the PBS was in the field of spacecraft to produce a cladding that can resist temperatures above 1500 °C (see Figure 2.8). [10], [8]

Figure 2.8.: Applications of PBS: (a) As rheological liquids; (b) for the manufacture of protection against mechanical damage; (c) as fire-resistant ceramics; (d) as self-healing material [8]

In addition, this material has also been used in shock protection systems and body armor protection. For example, Xu et al. [59] fabricated a sandwich structure with a core made of PBS and calcium carbonate ($CaCO_3$) additive and layers of Kevlar for a bulletproof vest, shown in Figure 2.9. This work aimed to study the influence of $CaCO_3$ percentage on the maximum energy dissipation. They conclude that adding PBS and $CaCO_3$ improves the energy dissipation by 60 %. more than neat Kevlar [20]. Another investigation made a shock transmission system (STU) filled with PBS for anti-seismic purposes Figure 2.10. For this purpose, they fabricated two prototypes of STU and tested them under different situations to observe their performance. The conclusion was that adding PBS to this device enables free motion under slow mechanical stresses, but it behaves as a solid elastic under impacts or seismic episodes.
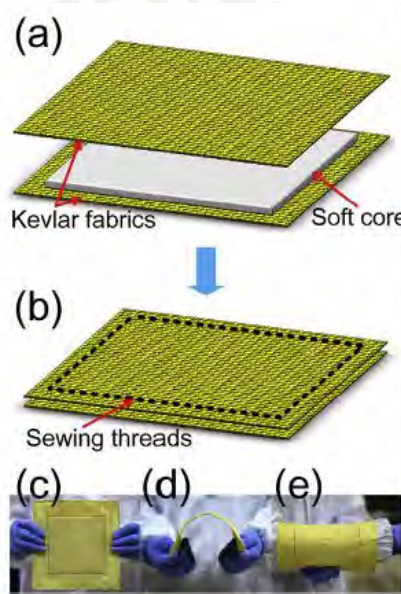
Figure 2.9.: Representation of the sandwich structure of PBS core and Kevlar layers [59]
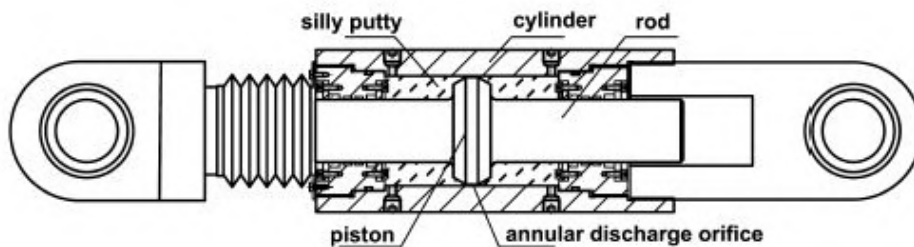
Figure 2.10.: Scheme of the shock transmission unit design [20]

In another investigation, Li et al. [19] explored the potential use of magnetic putty (Silly Putty with magnetic fillers) in the field of soft robotics. For this purpose, they examined

the morphology, composition, and rheology of pristine PBS, emphasizing its unique properties such as autonomous self-healing, malleability, and recyclability. Additionally, they added Neodymium-Iron-Boron (NdFeB) microparticles in various weight percentages into the pristine PBS to create magnetic PBS. To compare both samples, they characterized them through amplitude and frequency sweep tests. Furthermore, they assessed the remanence, coercivity, and retention of the magnetic PBS when a magnetic field is applied at different intensities. The investigation concluded that the magnetic force provided by a permanent magnet has the capacity to alter the geometry of magnetic PBS (see Figure 2.11). Moreover, when the external magnetic field is removed, this sample retains its deformation. The frequency sweep test indicated that magnetic PBS exhibits a larger storage modulus than loss modulus at higher shear rates, suggesting a more elastic behavior over time. Finally, the investigation concluded that this composite, after demagnetization, only requires an external magnetic field of $100\,\text{mT}$ to remagnetize it.
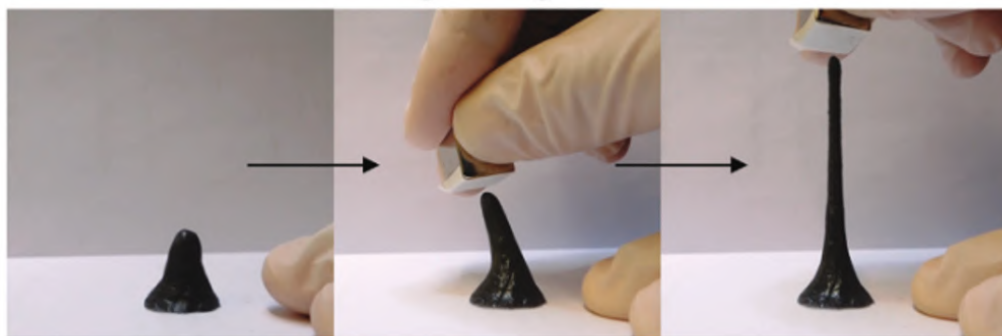
Figure 2.11.: Response of magnetic PBS to an external magnetic field [19]

2.3. Rheology of materials

According to Ramli Et al. [34], rheology studies the material's behavior (deform or flow) under different forces or stresses. This topic is important in applications such as material science, engineering, pharmaceuticals, and foods. For example, about polymeric paints, the rheology provides the information applications of these paints for brushing, spraying, and dipping. Another example is the rheology of melted polymers, which is important in different processes such as injection molding, extrusion molding, or fabrication of polymer-based composites.

2.3.1. Rheological behavior of materials

The rheological behavior of materials can be described by three categories: purely viscous where all the energy added is transformed into heat; purely elastic where all the energy added is stored in the material), and viscoelastic, which combines both effects. The last category cannot be

described by the simple models of hydrodynamics and elasticity. The most popular model to describe the flow behavior of these materials is the plate-plate model, shown in Figure 2.12. In this model, the upper plate moves with a velocity of V_p in the z-direction, while the lower plate remains static. As the figure shows, the velocity profile is not constant and depends on the distance between these two plates, where the maximum value is H. The force F is applied to the upper plate and causes the velocity V_p as well as a shear stress τ (see Equation 2.1). Also, the shear rate can be defined by the deformation of the liquid particles, which is the derivative of the velocity over the gap height. For this model, it results in the relation between V_p and the maximum distance H (see Equation 2.2). [5]
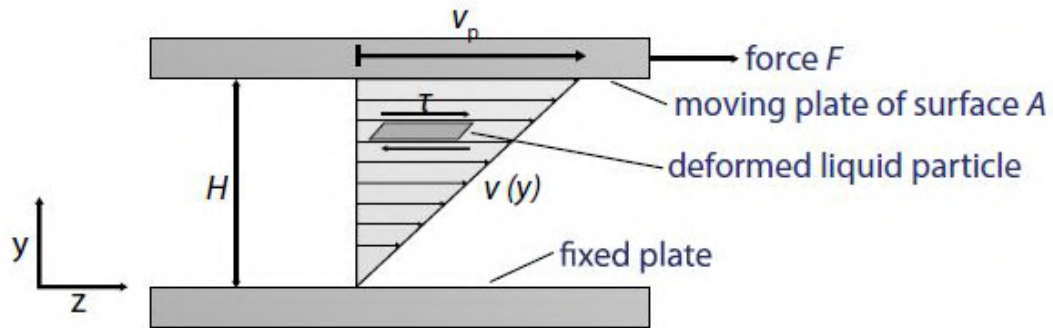
Figure 2.12.: Two-plate model with drag flow [5]

$$\tau = \frac{F}{A} \tag{2.1}$$

$$\dot{\gamma} = \frac{\partial v}{\partial y} = \frac{V_p}{H} \tag{2.2}$$

With the shear stress and shear rate, the viscosity can be defined by the flow resistance and the it is the division of τ and $\dot{\gamma}$ it has the unit of $\mathrm{Pa\,s}$ (see Equation 2.3).

$$\eta = \frac{\tau}{\dot{\gamma}} \tag{2.3}$$

Four different fluid behaviors can be described by the graphic of viscosity η and shear rate $\dot{\gamma}$, shown in Figure 2.13. The first is the Newtonian fluid (e.g., water), which has a constant viscosity value through the shear rate. The second is the pseudoplastic or shear-thinning fluid (e.g., Ketchup), where its viscosity decreases at higher shear rate values. This type of fluid possesses three zones: Newtonian zone, transition zone, and pseudoplastic zone. The third

type is the dilatant or shear thickening fluids (e.g., suspension of sand in water). These fluids are the opposite of pseudoplastic fluids because their viscosity increases at higher shear rate values. The last fluid is the Bingham fluid, which needs to reach a critical value of shear stress to start flowing. An example of this fluid is the toothpaste because it has an infinite viscosity until it reaches the critical shear stress. [38]
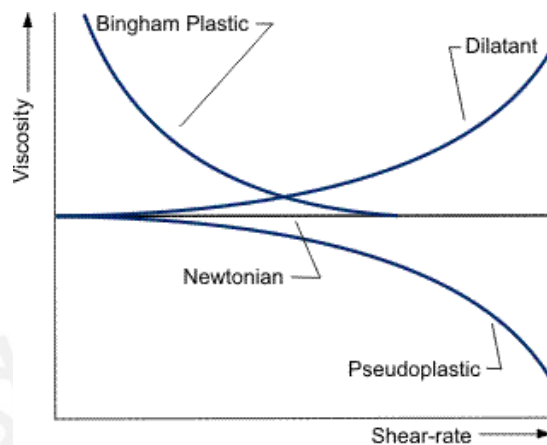
Figure 2.13.: Comparison of the viscosity behavior of four type of fluids [38]

2.3.2. Viscoelasticity of materials

Other important property of the polymers is the viscoelastic property, which results from the materials microscopic relaxation processes and intermolecular interactions. As explained above, it can be described by different responses, shown in Figure 2.14: Elastic, which does not have energy dissipation; Visco-plastic, which has an irreversible deformation and a dissipation of the potential energy into heat; Viscous materials, which transform all the potential energy into heat and deformation and viscoelastic materials that are in the middle of the conversion of the potential energy and complete recovery. These behaviors can be explained by two physical moduli, which are the storage modulus G' and loss modulus G", as shown in Figure 2.14. The first is related to the reversibly deformation (elastic) and the recovered energy and the second is related to the remaining energy transformed into heat. [40], [7]
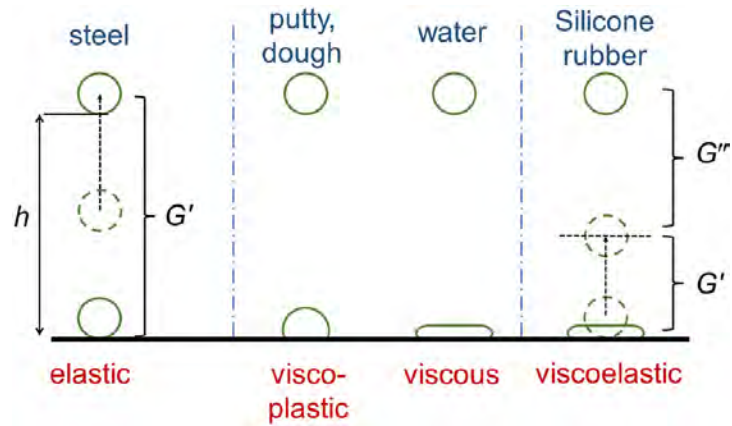
Figure 2.14.: Response of different types of matter on a deformation. Ideal elastic response, irreversible plastic deformation, viscous flow and viscoelastic response [34]

Many mathematical models can describe the viscoelastic behavior of different polymers, shown in Figure 2.15. These enable a relation between the data of the experiments and mathematical equations which are useful for simulations. The viscous behavior can be described by a damper by the Newton's law and the elastic behavior by a spring (Hooke's law). These two devices can be combined in a parallel or serial arrangement to obtain new models that predict in a more precisely way the viscoelastic behavior. One of them is the Maxwell model which consists in a series arrangement of damper and a spring. The other model is the Voigt-Kelvin model, which consists on a parallel array of a damper and a spring. However these models cannot fit the PBS behavior due to their solid and viscous fluid behavior which depends on the stress rate. A better model, that describes the viscoelastic behavior of PBS is the four parameter model due to the combination of two series systems that provide the PBS's solid and viscous fluids behavior. [13], [34]
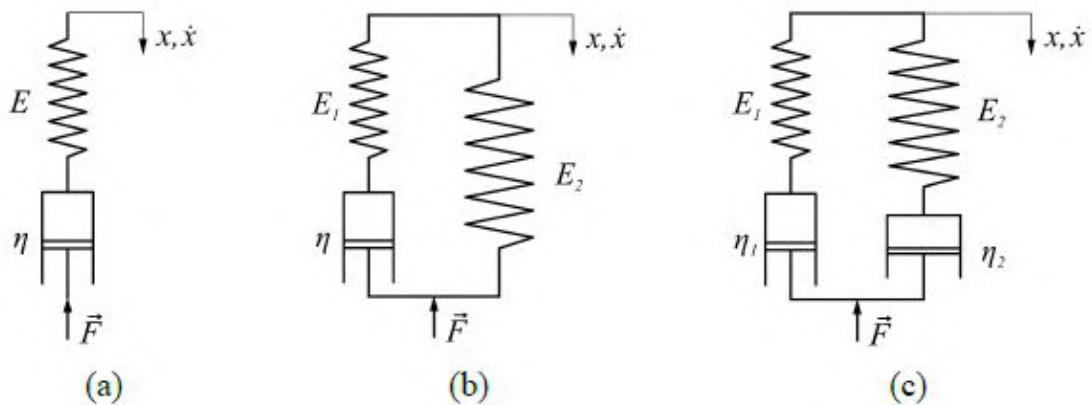
Figure 2.15.: Rheological models for viscoelastic materials: (a) Maxwell model; (b) Three parameter model; (c) four parameter model [13]

15

Regarding PBS viscoelastic behavior and its relation with the mentioned mathematical models, Tang et al. [49] investigated six PBS samples using PDMS as a precursor with different viscosities in toluene at 120°C to avoid complications during the fabrication process. They named these samples PBS1, PBS2, PBS3, PBS4, PBS5, and PBS6, where PBS1 was made with the lowest viscous PDMS, and PBS6, with the highest. These samples were characterized by a dynamic oscillatory frequency sweep from 0.1 to 500 $\frac{\text{rad}}{\text{s}}$ at 25 °C. They used the Maxwell model to understand the relaxation behavior of PBS following the equations 2.4 and 2.5, where $G_{e,fit}$ and τ_e correspond to the Plateau elastic modulus and the relaxation time for the slow-relaxed network structure, respectively, and $G_{b,fit}$ and τ_b correspond to the elastic modulus and the relaxation time for the fast-relaxed supramolecular structure. The curves from the Maxwell model and the experimental curves are represented in Figure 2.16. These curves show that the Maxwell model fits well for PBS1 (low viscosity precursor), but for PBS6 (high viscosity precursor), these curves have a significant error, especially for values above the crossover point.

$$G' = \frac{G_{e,fit}\omega^2\tau_e^2}{1+\omega^2\tau_e^2} + \frac{G_{b,fit}\omega^2\tau_b^2}{1+\omega^2\tau_b^2} \tag{2.4}$$

$$G'' = \frac{G_{e,fit}\omega\tau_e}{1+\omega^2\tau_e^2} + \frac{G_{b,fit}\omega\tau_b}{1+\omega^2\tau_b^2} \tag{2.5}$$
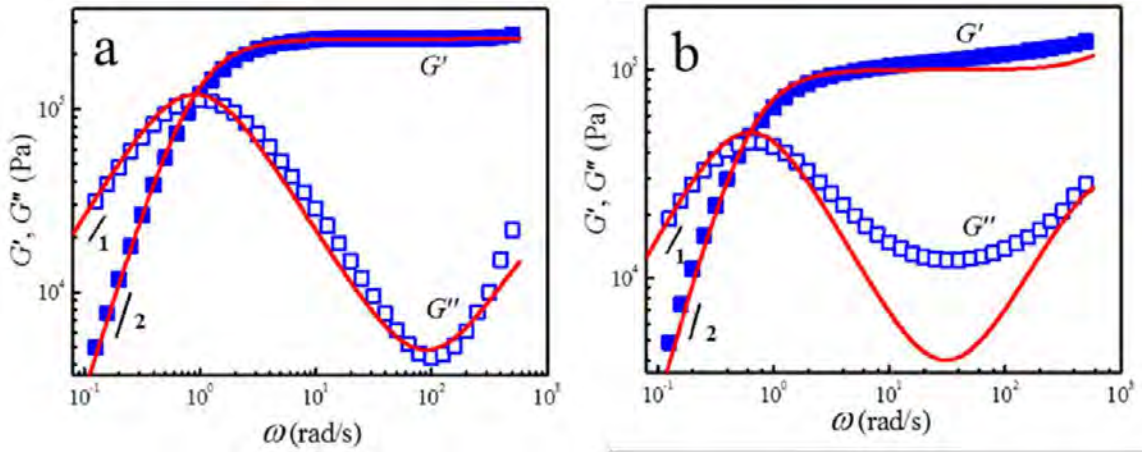
Figure 2.16.: Experimental curves and Maxwell model curves at 25°C: a) PBS1 ; b) PBS6. Solid red lines corresponds to the Maxwell model curves [49]

2.3.3. Methods for measuring rheological properties

There is variety of testing devices for rheological material characterization. However, the rotational rheometer is the most common because it can be used for different tests such as viscosity, amplitude, or frequency sweep tests. This device consists of two plates (upper and bottom plate), which are equipped with a sensor, shown in Figure 2.17. The upper plate oscillates rotationally while the bottom plate remains static during the test. This oscillation of the upper plate depends on the set strain or amplitude and angular frequency. In addition, the sensor of the upper plate detects the strain of this geometry γ, called angle of torque. The second sensor measures the counter torque on the lower plate which is a reaction of this geometry to keep it in position and is recorded as shear stress σ. These signals are represented by sine curves shown in Figure 2.18, where the graphic corresponds to the typical response of a viscoelastic material. [17]

Commonly, the measured parameters in this device are the storage modulus G', loss modulus G" and the relation between they can be described by the complex modulus G*, phase angle δ, or the tangent of the phase angle tanδ, shown in Figure 2.19. This complex modulus are calculated by the ratio of the applied strain and the measured stress as is shown in Equation 2.6. [17]

$$G* = \frac{\sigma_{\max}}{\gamma_{\max}} \tag{2.6}$$
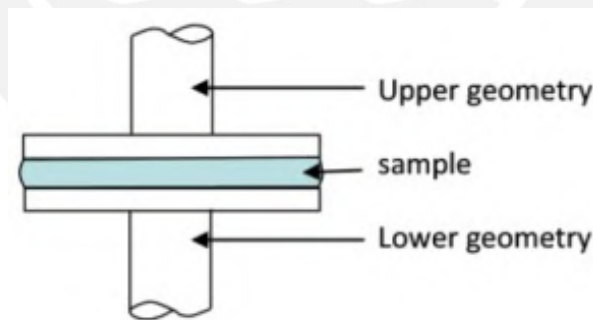
Figure 2.17.: Scheme of a plate-plate rheometer [54]
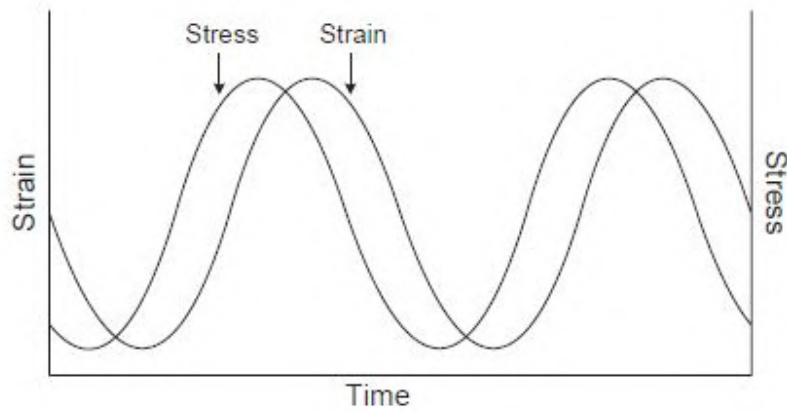
Figure 2.18.: Oscillation stress/strain waves for purely elastic and viscous materials [17]
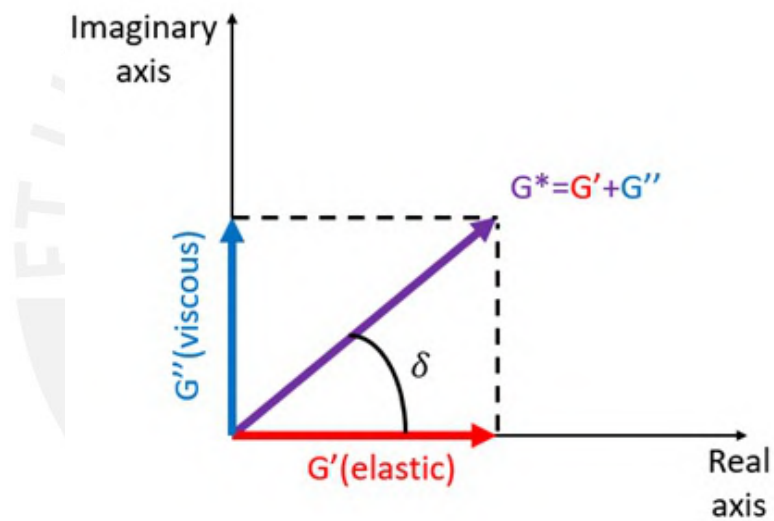
Figure 2.19.: Vectorial scheme of G* and their components in the real and imaginary axis. Adapted from [23]

3. Critical review and intended goals

The exploration of various categories of smart materials and their applications in diverse areas, such as medicine, energy harvesting, and robotics, was presented in the previous chapter. However, these smart materials exhibit significant deficiencies for advanced developments , such as in soft robotics. These limitations encompass challenges related to transitioning between fluid and solid states, achieving malleability, and incorporating self-healing capabilities within a single material. Such properties are crucial for applications in grippers or locomotion systems, enabling them to adapt to different surfaces or environments. For example, shape memory alloys can memorize specific geometries, but their higher stiffness compared to silicon makes them overly complex for use in human-robot interactions. This enabled a growing interest in polyborosiloxanes (PBS), a material with the capability to transition from a viscous fluid to a rubbery solid, a behavior highly influenced by its chemical structure and supramolecular interactions.

Numerous investigations have aimed to understand the influence of different factors during PBS synthesis on its behavior. While some studies focused on the impact of temperature and precursors, others examined variations in the viscosity of PDMS and its hydroxyl groups. Additionally, other researches has explored the effects of magnetic fillers on PBS characteristics, such as shear stiffening capacity, self-healing properties, and shapeability under external magnetic fields. However, a research gap persists, as no studies have explored the distinctions between mixing different PDMS precursors or PBS samples and their influence on mechanical and rheological properties. Moreover, although external magnetic fields have been studied as stimuli for PBS, there is a dearth of evidence regarding the influence of vibrations on its mechanical properties and shape retainability.

For these reasons, the principal goal of this investigation is to study the influence of diverse mixing ratios of two PDMS precursors with different viscosities on the rheological properties, emphasizing the differences between mixing two PDMS precursors or two PBS samples. Additionally, this investigation evaluates the influence of mechanical stimuli (vibrations) at different frequencies on the shape retainability of PBS and its flow behavior. Addressing these research goals will provide valuable insights into the behavior of PBS using different mixing methods and ratios, offering initial approaches to PBS applications in soft robotics and enhancing their adaptability and performance under various conditions.

To achieve these goals, a synthesis procedure for PBS is defined based on a previous investigation, with the aim of fabricating homogeneous PBS and avoiding complications that could affect its properties. [33] Two PDMS precursors with significant differences in viscosities (45-85 and $750 \cdot 10^{-6} \, \frac{\text{m}^2}{\text{s}}$) are selected to observe their influence on PBS properties. Following

the fabrication process, the samples were tested by Fourier Transform Infrared Spectroscopy and Raman Spectroscopy to analyze the chemical bonds present in their structure, enabling a comparison with other PBS samples from separate investigations. Morphological characterization is employed to evaluate the PBS surface and identify any unreacted components resulting from the synthesis process. Additionally, a thermogravimetrical characterization is performed to determine the maximum working temperature, decomposition temperature, and assess the thermal stability of different components present in PBS. For rheological characterization, an amplitude and frequency sweep test is conducted, considering parameters from previous investigations. [18], [49] Finally, a shape change test is executed at various frequencies to observe PBS deformation over 150 minutes and study its shape retainability.

4. Experimental Methodology

This section defines the experimental methodology to achieve the objectives of this investigation. First, this chapter describes the synthesis process for fabricating the PBS samples including the materials, instruments and the followed manufacturing process. Then, it explains a brief background of each characterization tests and their parameters.

4.1. Polyborosiloxane synthesis

As explained in the previous chapter, there are many synthesis processes to obtain polyborosiloxane with different characteristics, which depend on each investigation's application or aim. In this work, the objective is to characterize the PBS analyzing the influence of different PDMS precursors on PBS properties. For this reason, is important to avoid chain scissoring during the synthesis, which will affect on the mechanical properties of the samples. [64] The fabrication process follows the investigation of Reuss [36], which consists in reacting BA and PDMS as precursors at temperatures below $150\,°\text{C}$, avoiding random chain scissoring.

4.1.1. Materials

A) Polydimethylsiloxane (PDMS)

Two different PDMS precursors are used for the PBS synthesis: PDMS1 from Merck (Sigma-Aldrich) with a viscosity of $45\text{-}85 \cdot 10^{-6}\,\frac{\text{m}^2}{\text{s}}$ and PDMS2 from acbr GmbH with a viscosity of $750 \cdot 10^{-6}\,\frac{\text{m}^2}{\text{s}}$ (see Figure 4.1). Both precursors have hydroxyl groups (OH) in different quantities to obtain the characteristic dynamic bonds of PBS, which are also related to the viscosity of each precursor. [45], [1]

B) Boric Acid (BA)

The second precursor is the Boric Acid, a weak monobasic Lewis acid of boron with the chemical formula of H_3BO_3. Mostly, it is used for processing and manufacturing pharmaceutical products or cosmetics. For this investigation, the Boric Acid has a purity of $99.5\,\%$ and is from the company Sigma-Aldrich, shown in Figure 4.2. [44]
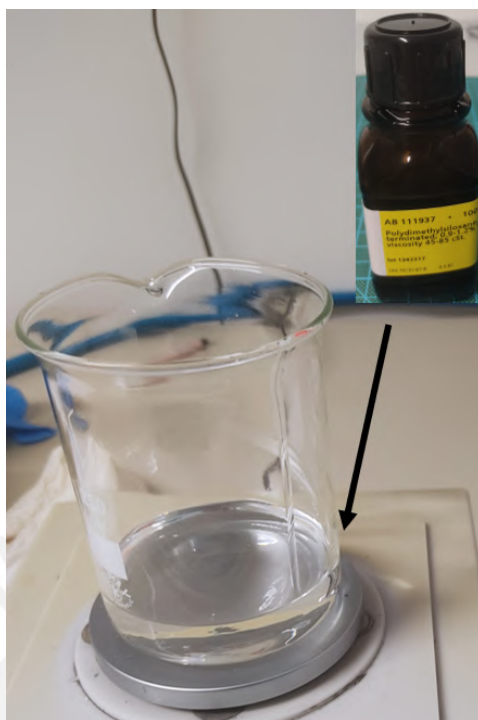
Figure 4.1.: Polydimethylsiloxanes precursor used for the PBS synthesis
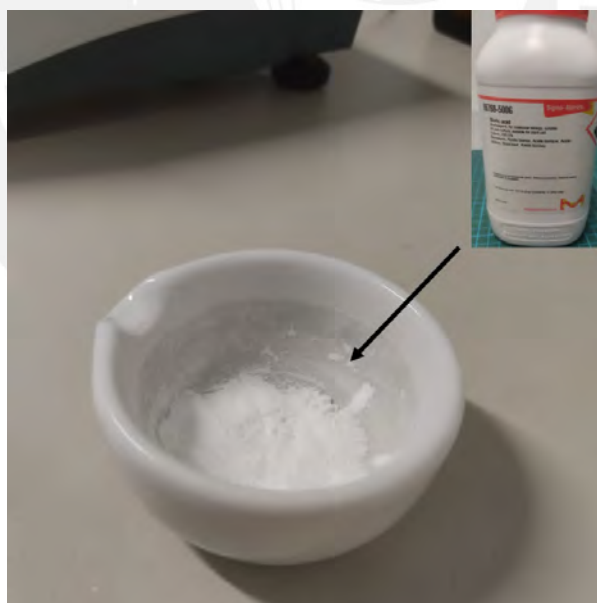
Figure 4.2.: Boric Acid precursor from Sigma-Aldrich company

4.1.2. Instruments

The temperature during the PBS synthesis must be controlled to prevent boric acid sedimentation and achieve a homogeneous material. To monitor this, a digital thermometer Greisinger GTH 175PT equipped with a pt1000 probe is employed. [12] Additionally, the mixing process of PDMS and BA requires constant stirring for a successful synthesis. To solve this requirement, a magnetic stirrer model Guardian 3000 from the company Ohaus is utilized, with a maximum heating capacity of $380\,^{\circ}\mathrm{C}$ and a maximum stirring capacity of $1600\,\mathrm{rpm}$. [29] Finally, the PBS synthesis involves a condensation reaction that results in water molecules within the structure. To evaporate and eliminate these molecules, the samples need to be dried at temperatures up to $100\,^{\circ}\mathrm{C}$. For this purpose, a forced convection oven BINDER FD53 is employed, featuring a temperature range from $5\,^{\circ}\mathrm{C}$ to $300\,^{\circ}\mathrm{C}$ and an integrated timer with a duration of up to 99.59 hours. [52] The experimental setup, including all the instruments used in the PBS synthesis process, is shown in Figure 4.3.
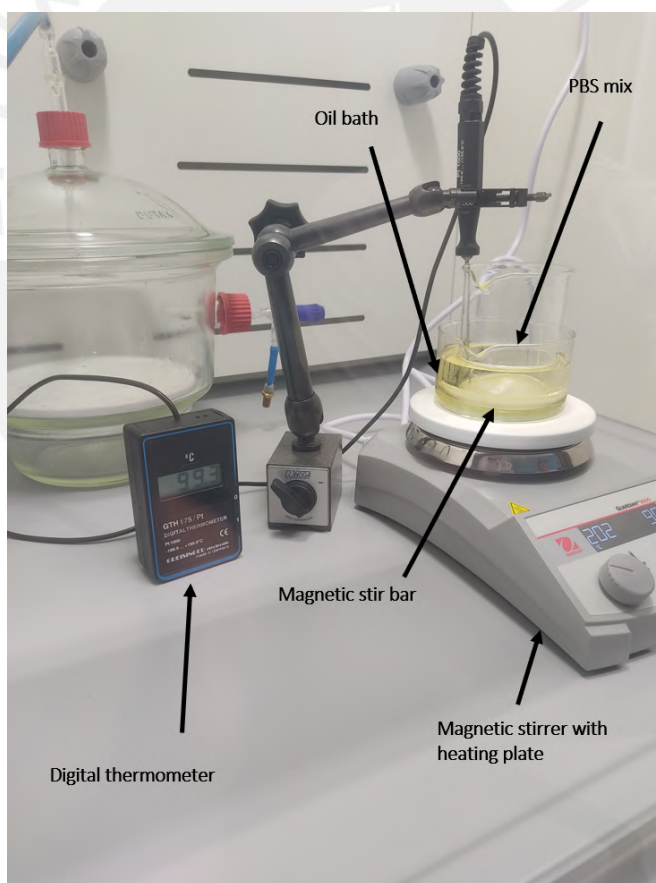
Figure 4.3.: Setup for the PBS synthesis

4.1.3. Samples fabrication

The procedure for fabricating PBS samples is defined based on a prior investigation [33], following the synthesis method proposed by Reuss in 2016. [36] The temperature and rotational velocity during synthesis are chosen to reduce the viscosity of the mixture and prevent Boric Acid sedimentation. Moreover, the polymerization of PBS results in the splitting of water molecules, contributing to an increase in viscosity and affecting its rheological properties. To address this, the samples were dried after the reaction, facilitating the evaporation of these molecules.

Based on the objective of this thesis, the PBS samples are categorized into three groups: Pure PBS samples, Pre-Mixed PBS samples, and Post-Mixed PBS samples. The following lines outline the steps taken to generate approximately 20 grams of PBS in each category.

1. weight the proper quantities of PDMS ($20\,g$) and BA ($0.62\,g$);

2. mix both precursors in a beaker using a glass rod or a spoon;

3. immerse the beaker in an oil bath to obtain a homogeneous temperature in the mix and maintain a temperature of $100\,°C$ during the synthesis;

4. put the stirring bar inside the beaker and set a speed of 50 to 200 rpm depending on the viscosity of the mix. Check the mix constantly to avoid sediments of BA;

5. the mixing process concludes either when the viscosity of the mixture abruptly increases or when the mixture wraps around the stirrer, resulting in the stirring bar no longer rotate;

6. move the mix to a heat-resistant glass and put it inside an oven at $130\,°C$ for 24 hours to evaporate all the water product of the synthesis.

A)Pure PBS samples

The pure PBS samples follow the next nomenclature: PBS1 made with PDMS1 ($45\text{-}85{\cdot}10^{-6}\,\frac{m^2}{s}$) and PBS2 made with PDMS2 ($750 \cdot 10^{-6}\,\frac{m^2}{s}$). For pure PBS samples, the synthesis process follows the steps mentioned above. The dried synthesized samples are shown in Figure 4.4, where the bubbles of the image corresponds to the evaporated water molecules after the drying process.
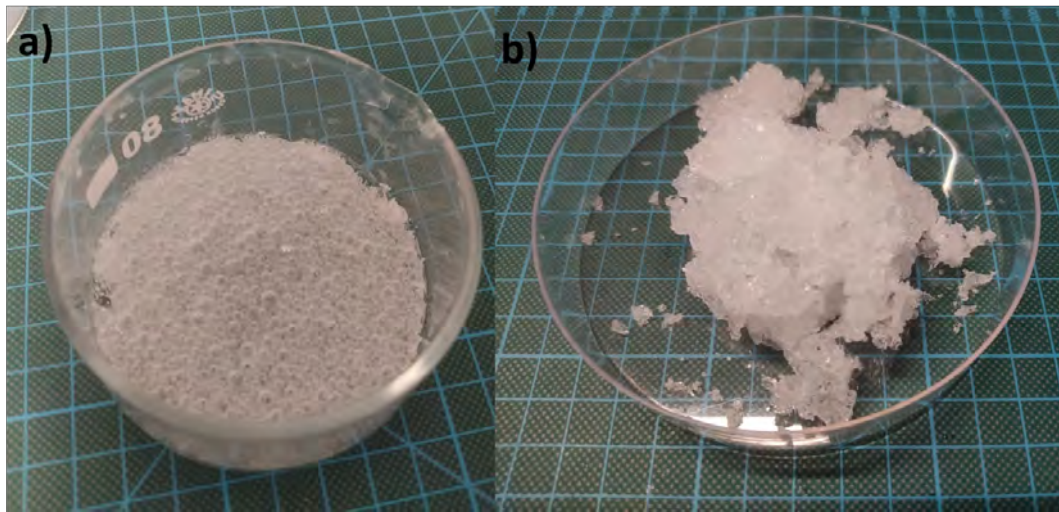
Figure 4.4.: a) PBS sample after 16 hours of drying ; b) PBS sample after 24 hours of drying process, where the material exhibits a brittle behavior

B) Mixed PBS samples by mixing two PDMS precursors

For these samples, a pre-mixing step is introduced where PDMS1 and PDMS2 are combined before the addition of boric acid (BA) to the synthesis process. This pre-mixing is crafted using different mixing ratios of 20/80, 40/60, 60/40, and 80/20 % in mass. These resulting PBS samples is referred to as "Pre-mixed PBS." This nomenclature emphasizes the stage at which the mixing occurs before the synthesis process, making it clear to distinguish these samples from others in the study.
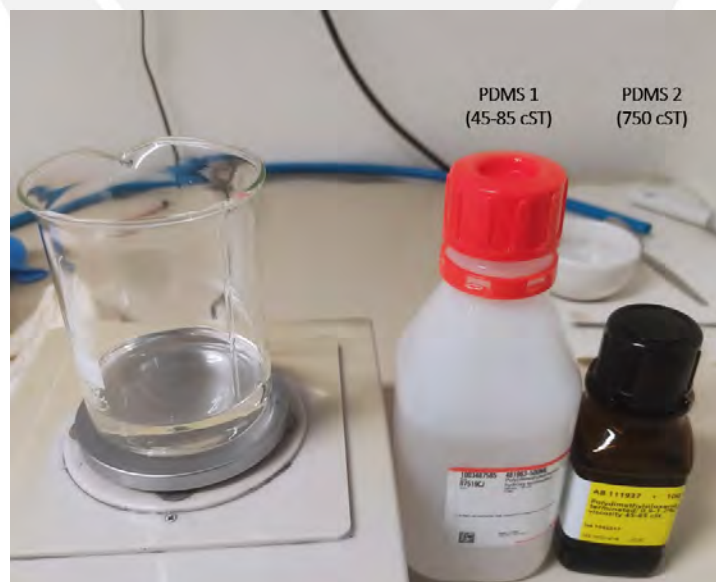
Figure 4.5.: Mixing process of PDMS1 and PDMS2

C) Mixed PBS samples by mixing two pure PBS samples

For the "Post-mixed PBS" samples, the process involves combining pure PBS1 and PBS2 following mixing ratios of 20/80, 40/60, 60/40, and 80/20 % in mass. These samples are mixed by passing them through a roller mill for 10 times, ensuring complete homogeneity, as is illustrated in Figure 4.6. This nomenclature emphasizes that the mixing occurs after the individual synthesis of PBS1 and PBS2, providing clarity in categorizing these samples in the study.
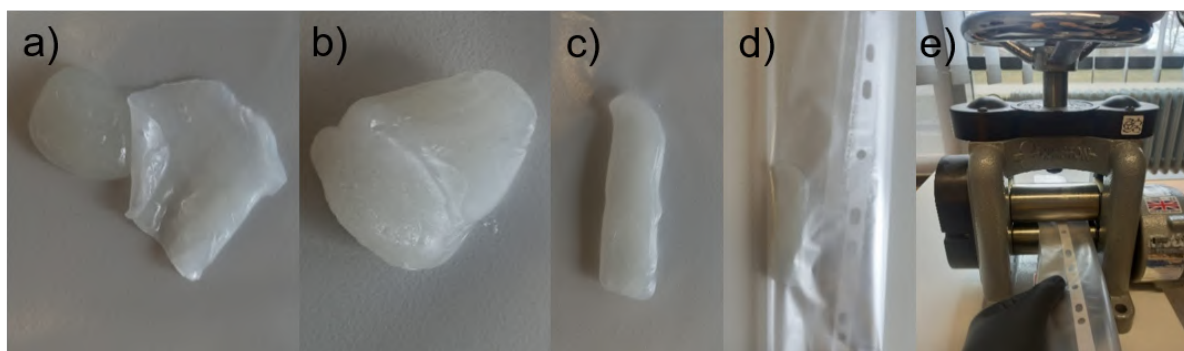
Figure 4.6.: Fabrication process of Post-mixed PBS samples using a roller mill: a) weigh the proper quantities of PB1 and PBS2; b) manually mold both PBS into a linear geometry; c) roll the mixture; d) place the mixture into a film to prevent contamination during rolling; e) pass the film through the roller mill

4.2. Chemical characterization

4.2.1. Fourier Transform Infrared Spectroscopy (FTIR)

Fourier Transform Infrared Spectroscopy (FTIR) is a chemical characterization technique that provides information about different chemical groups, chemical bonds, or functional groups present in the material's structure. It can be used to analyze small or complex molecules in cells or tissues. This test consists of the emission of infrared radiation through the material sample (see Figure 4.7). The sample absorbs some of this emitted radiation, and the other is transmitted, which results in different characteristic peaks of the chemical structure. In this investigation, this test confirms the correct synthesis of PBS, comparing the obtained FTIR spectra of synthesized PBS sample with the PBS spectra of other investigations. [4]

The principle of this test is associated with the molecular vibrations of the functional groups. Each group has a fundamental vibration related to the infrared absorption bands provided by the FTIR test. This technique detects only the molecules' asymmetrical vibrations, which limits its sensibility at some wavelengths. For this reason, some investigations combine this test with Raman Spectroscopy to obtain a wide range of analyses. [39], [9]
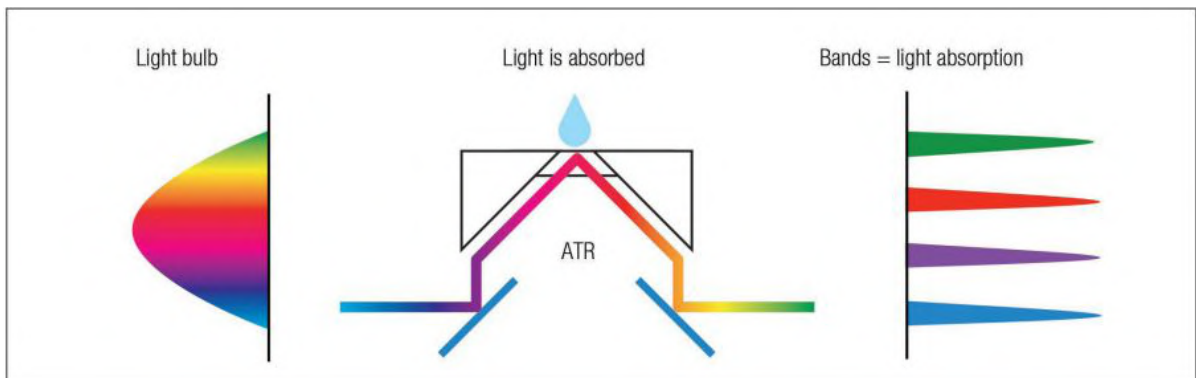
Figure 4.7.: Visual Representation of FTIR principles. [53]

The Bruker Tensor 27-FTIR spectrometer, depicted in Figure 4.8, was utilized for this test. It is based on an Attenuated Total Reflectance (ATR) method, employing a high-refractive-index prism made of diamond, zinc selenide (ZnSe), or germanium (Ge) to measure the reflected infrared light from the sample and obtain its characteristic spectra. Moreover, this device has a spectral range of 7500 to 370 cm^{-1} and a resolution of 1 cm^{-1}. The test followed the ASTM-E1252 standard, employing a spectral range from 4000 to 400 cm^{-1}, consistent with the study conducted by Kurkin et al. [18] The details of the parameters applied in this test are presented in Table 4.1. [42], [46]
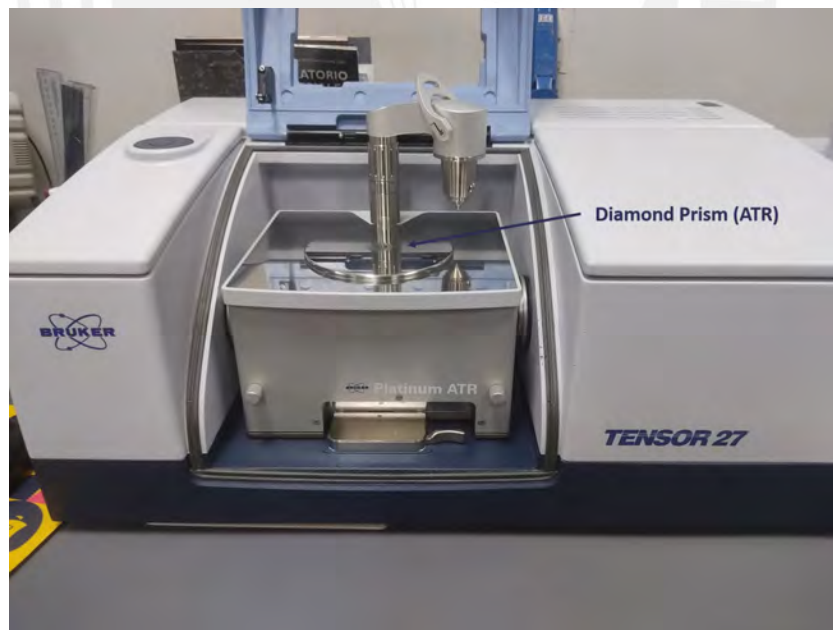
Figure 4.8.: FTIR spectometer Bruker Tensor 27

Table 4.1.: FTIR test parameters

Parameter	Value
Spectral range (cm^{-1})	4000-400
Resolution (cm^{-1})	0.1
Number of scannings	64
Type of detection	Absorbance

4.2.2. Raman Spectroscopy

Similar to the FTIR, this test provides information about the molecular interactions present in the structure of the sample, providing a "chemical fingerprint" of it. In this technique, a single wavelength laser is projected to the sample (See Figure 4.9). When this laser passes through the material, it divides into scattered light, which is measured and provides spectra. In contrast to FTIR, Raman spectroscopy detects the symmetric vibrations of the molecule, which provides the ability to distinguish between single, double, or triple bonds. In combine with FTIR, this test provides the necessary information to confirm the correct synthesis of PBS and different chemical bonds that can be present in PBS samples. [9], [53], [35]
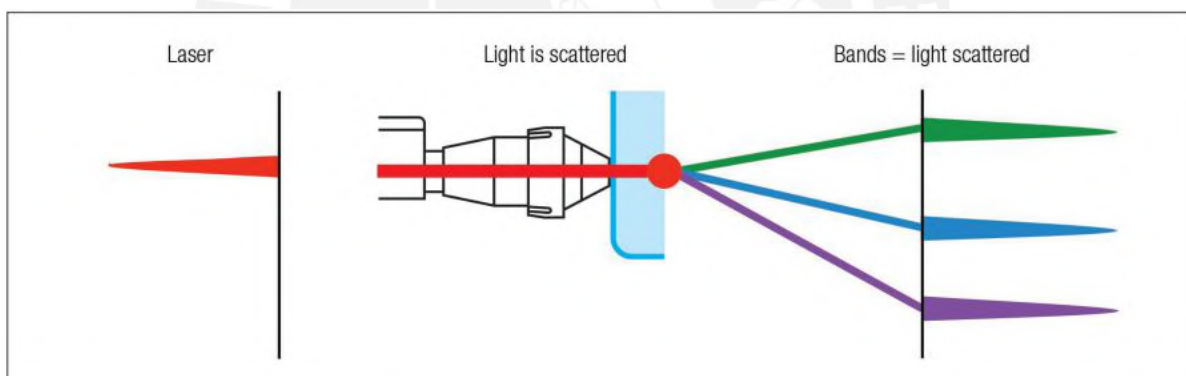
Figure 4.9.: Visual Representation of Raman Spectroscopy principles [53]

The test was performed using a range of wavenumber of 100 to 3200 cm^{-1} and 10% of the total power of the laser. The sample was tested by the Raman spectrometer and microscope Renishaw inVia (see Figure 4.10) and the parameters are shown in Table 4.2.

Table 4.2.: Raman spectrometry parameters

Parameter	Value
Spectral range (cm^{-1})	100-3200
Laser power $(\%)$	10
Exposure time (s)	15
Objective (magnifications)	x50
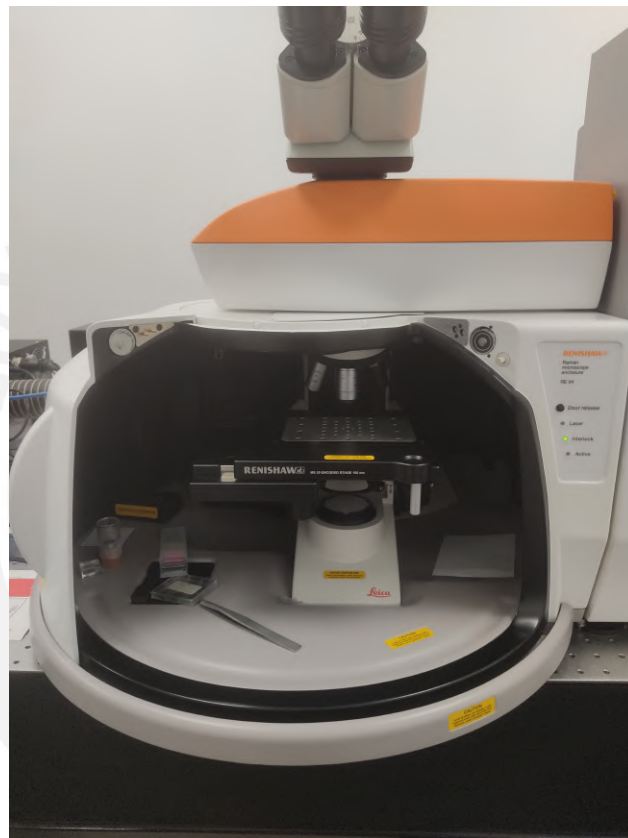
Figure 4.10.: Raman spectometer and microscope Renishaw inVia

4.3. Morphological characterization

4.3.1. Scanning Electron Microscopy (SEM)

Scanning Electron Microscopy (SEM) is a technique for obtaining high-resolution images and detailed surface information of various samples. Its resolution range can reach from less than 1 nanometer to several nanometers. Unlike optical microscopes, which are based on light, SEM uses a focused beam of high-energy electrons over the sample and reads the different signals produced by the interaction of the electron and the sample. [25] In this investigation, SEM test

provides information of the surface of PBS samples and possible residual boric acid present in PBS structure.

This beam of electrons is produced by an electron source (gun) and conducted by an arrangement of different lenses in an environment of vacuum (see Figure 4.11). When the beam impacts the sample, it emits signals such as X-rays, secondary electrons, and primary backscattered electrons that detectors absorb. These signals are processed using a scan generator and an amplifier to obtain the final image. [31]
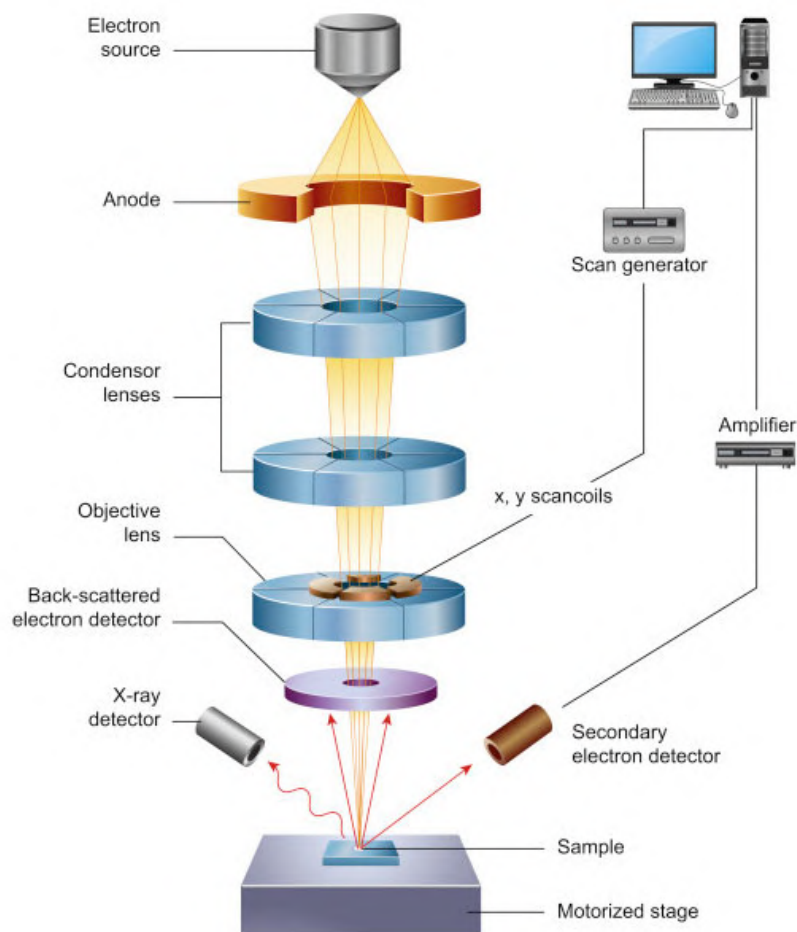
Figure 4.11.: Schematic of a scanning electron microscope [25]

4.4. Termogravimetrical characterization (TGA)

Thermal Gravimetric Analysis (TGA) is a technique used for characterize the thermal stability of the material at different temperatures and gas atmospheres. The procedure consists in a constant heating and measuring of the weight sample (gain or loss). The chosen atmosphere depends on the material of the sample and it can be an inert gas(nitrogen) or an oxidative

(oxygen). A representation of this process is shown in Figure 4.12, where is observed the inlet and outlet of the mentioned gases. This test provide important information of the material such as degradation temperature, maximum working temperature and some reactions that can occur because of the interaction between the sample and the atmosphere at specifics temperatures. Some parameters that are important for this test is the temperature range, the heating rate and gas atmosphere. [47], [30]
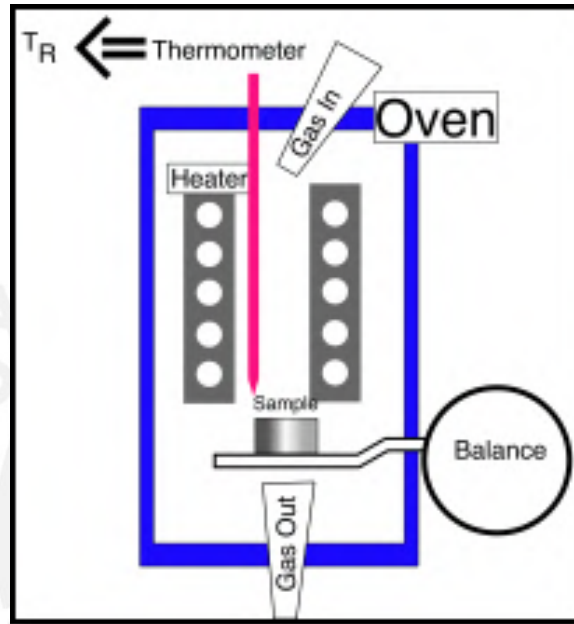
Figure 4.12.: Scheme of a TGA device

The TGA test in this investigation was performed in accordance with the ASTM E1131-08 standard, following the parameters listed in Table 4.3. The TGA analyzer used is the NET-ZSCH STA 449 F1 Júpiter®, shown in Figure 4.13. This device features a furnace with a capacity ranging from -150° to 2000 °C and a high-precision scale with a resolution of 0.025 µg. Both components are illustrated in Figure 4.14, displaying the reference and the sample. [28]

Table 4.3.: TGA test parameters

Parameter	Value
Temperature range (°C)	Ambient - 850
Heating range (°C/min)	10
Gas atmosphere (until 600°C)	Nitrogen
Gas atmosphere (until 850°C)	Oxygen
Gas flow rate (ml/min)	50
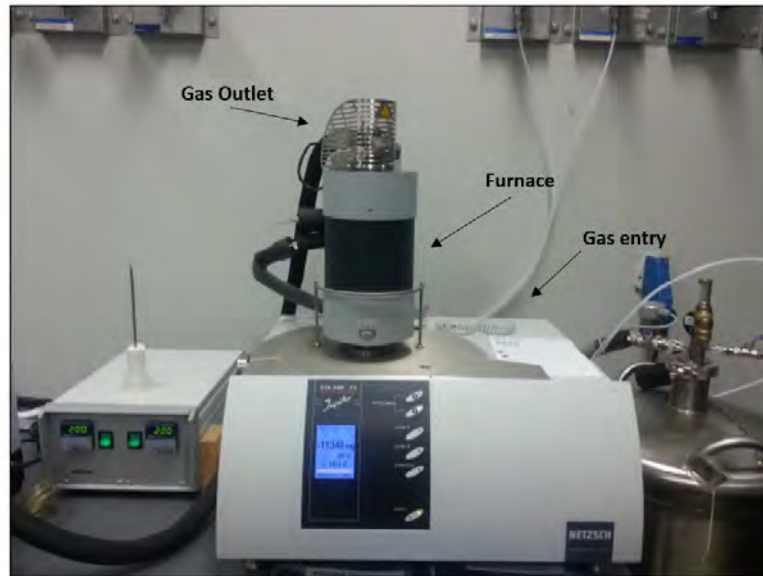
Figure 4.13.: Netzsch STA 449 F1 Jupiter®.
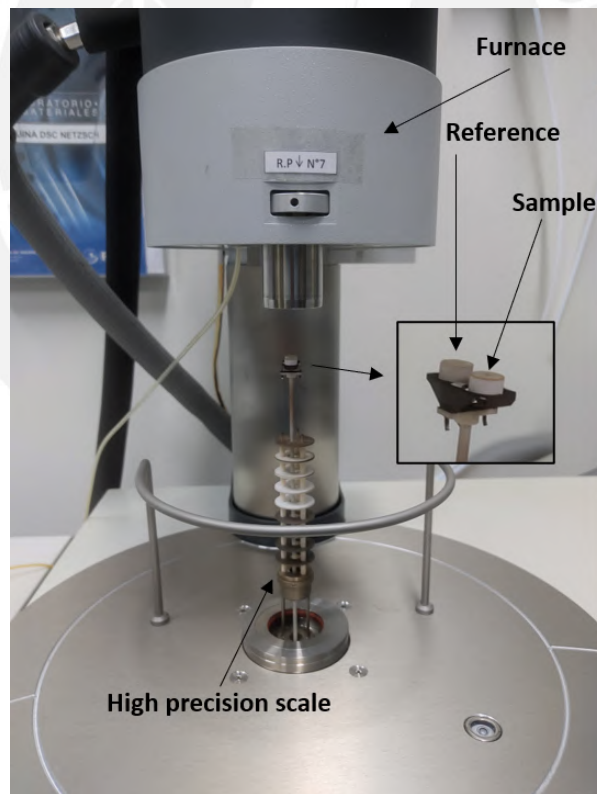
Figure 4.14.: Components of Netzsch STA 449 F1 Jupiter®.

4.5. Rheological characterization

4.5.1. Test instruments

The rheological tests were conducted using a rheometer, specifically the Netzsch model Kinexus Prime Pro+, as depicted in Figure 4.15. This device features a temperature capacity range from -40 to 450 °C, a torque range capacity from 1 nN m to 225 mN m, and the ability to perform various tests including viscosity tests, amplitude sweep tests, and frequency sweep tests. The rheometer employs an air pressure system regulated by valves (located on the right side) to achieve the operational pressure, preventing any malfunction during the test. [27]

Figure 4.15.: Rheometer Netzsch Kinexus Prime Pro+

Furthermore, this testing device uses a cryo-compact circulator model CF41 from Julabo to maintain each test's set temperature, shown in Figure 4.16. It has a capacity temperature range of -40 to 200°C and a temperature stability of ±0.02 °C. [16]

Figure 4.16.: Cryo-compact circulator Julabo CF41

The geometry used in this investigation was the plate-plate configuration with a diameter of 25 mm for both plates. The nomenclature of the upper plate is PU25 SR4285 SS, and the bottom plate is PL25 S3064 SS. The selected geometry is adequate for fluids with low viscosity to soft solids, which better describes the behavior of PBS. In addition, this geometry was used in a preliminary investigation of Reuss [36], where the results showed that the plate-plate and cone-plate configurations have similar measured data.
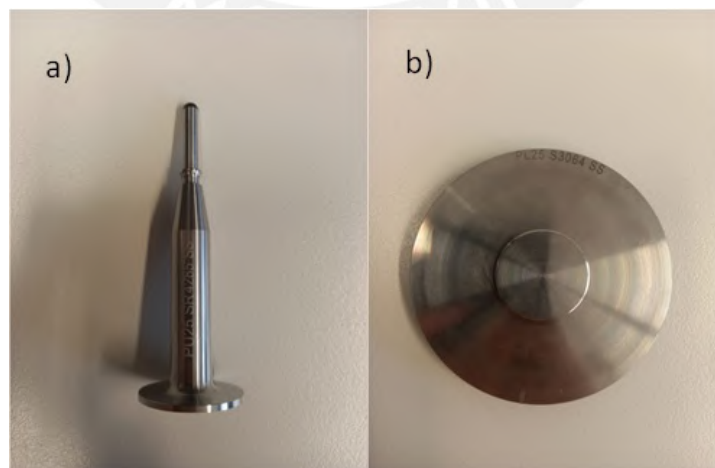
Figure 4.17.: Plate geometries used for amplitude and frequency tests. a) Upper geometry (plate ⌀25 mm); b) Bottom geometry (plate ⌀25 mm)

4.5.2. Samples preparation

In order to perform each test under the same conditions and reduce the error source, a preparation sample approach was defined. This sequence helps reach a homogeneous plain sample surface, which was prepared from experience during the preliminary investigation. [33] The mentioned procedure follows the next step that is shown in Figure 4.18.

a) extracting a little piece of the PBS and giving it the form of a layer with a thickness near the desired;

b) putting it on the lower geometry of the rheometer;

c) trimming the leftover material around the plate;

d) closing the active hood and start the test;

e) removing the material after the test is done.
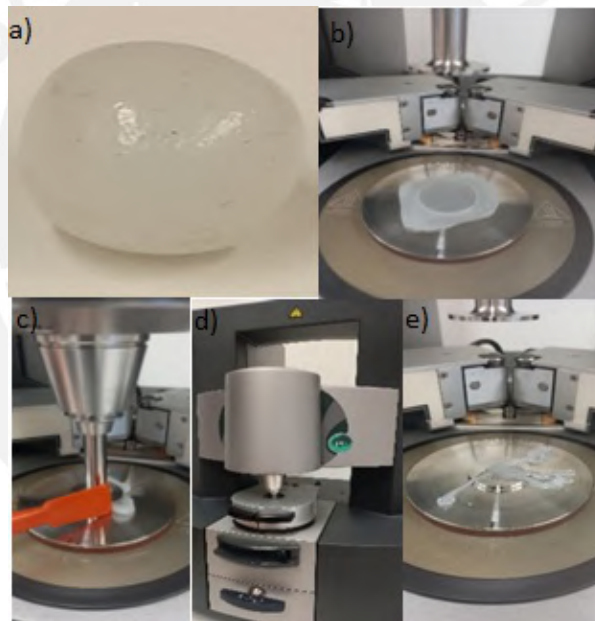
Figure 4.18.: Preparation process of samples before sweep tests (The letters follow the steps mentioned above)

4.5.3. Amplitude sweep test

The amplitude sweep or dynamic strain test consists of oscillating the plate, varying the amplitude in the set range at constant frequency and temperature. This test is useful to describe the behavior of many dispersions, pastes, and gels for use in food cosmetics or the medical industry. [7], [2]

This test allows us to obtain diverse material's Linear Viscoelastic Region (LVER). Inside this region, the applied stresses are insufficient to cause the structure's breakdown, and the sample conserves its original structure. The graphic result of this test shows the LVER region as a constant storage modulus G' throughout the time, and it ends when this value decreases suddenly. A representation of this event is shown in Figure 4.19. [26]

In addition, this test is required before the frequency sweep test if the information about the material's LVER is unavailable because, for the second test, the stress value has to be inside the LVER to avoid sample breakdown during the test. Commonly, the critical point of this zone is defined when the value decreases by 5 %. [37] The following parameters for this test are shown in Table 4.4.
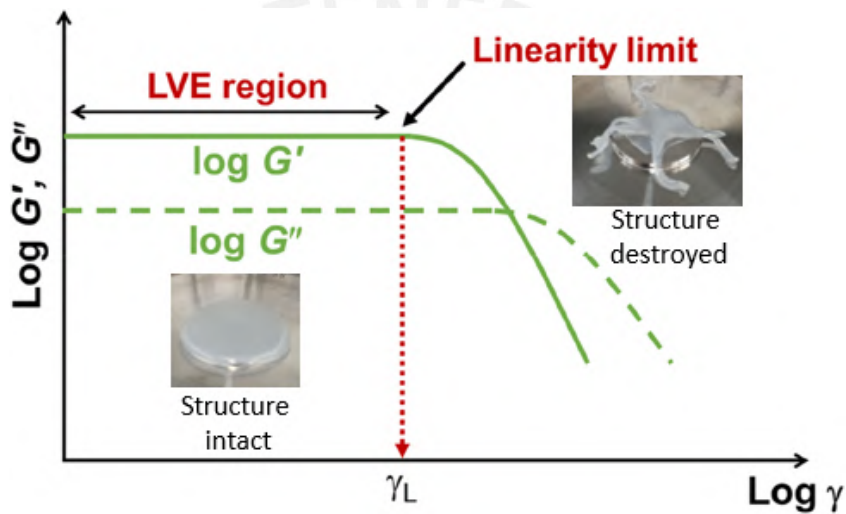
Figure 4.19.: Representation of LVER region obtained through amplitude sweep test [34]

Table 4.4.: Amplitude sweep test parameters

Parameter	Value
Shear strain (%)	0.01-100
Frequency (Hz)	16
Gap (mm)	1
Temperature (°C)	25

4.5.4. Frequency sweep test

The frequency sweep test describes the behavior of a material at different changes of stress or stress rates. Low frequencies correspond to low-stress rates, and high frequencies correspond to high ones. This test's amplitude value remains constant, whereas the frequency varies over time. [58]

This test provides information about the behavior of a viscoelastic material through a wide range of frequencies. Figure 4.20 shows a typical frequency sweep test result of PBS. At low frequencies, the dominant parameter is the loss modulus G", which indicates the viscous liquid behavior of this material. In contrast, the dominant parameter changes to the storage modulus G' at high frequencies, and the behavior changes to a viscoelastic solid. The gel point defines this behavior change where both curves have the same value. Furthermore, this test is useful to obtain viscoelastic properties such as stiffness (complex modulus), solid nature (storage modulus), liquid nature (loss modulus), solid or liquid tendency (phase angle), and complex viscosity. In this investigation, this test provides information of PBS shifting point (gel point), finding the frequency where the behavior of this material changes from viscous fluid to rubbery solid. [37] The followed parameters for this test are shown in Table 4.5.
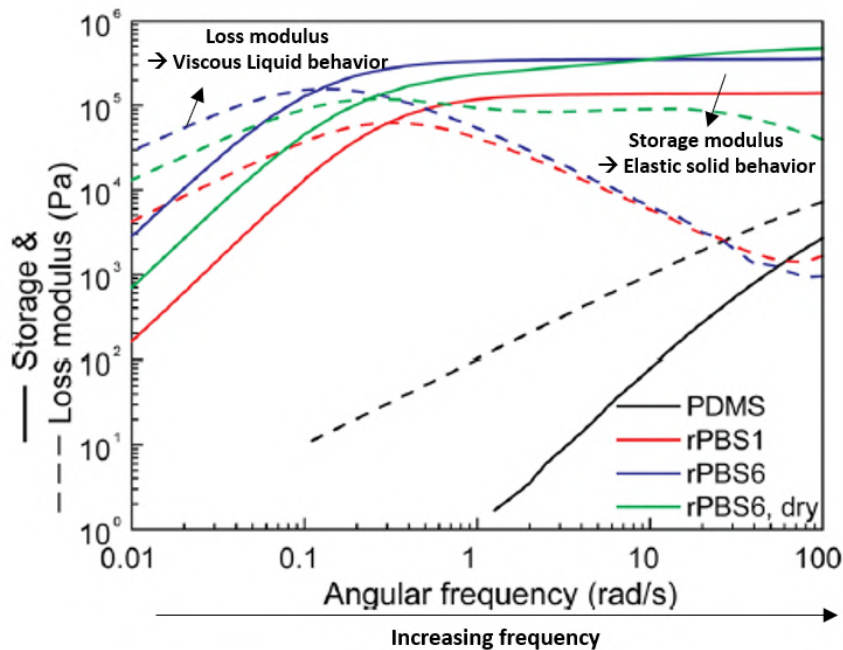
Figure 4.20.: Frequency sweep test curves of different PBS samples [67]

Table 4.5.: Frequency sweep test parameters

Parameter	Value
Shear strain (%)	0.1
Frequency (Hz)	0.01-100
Gap (mm)	1
Temperature (°C)	25

4.6. Shape change test

One of the objectives of this investigation is to provide the first approach for the PBS application in different systems for soft robotics, such as grippers and locomotion. For this reason, this test aims to characterize the influence of different stimuli in the shape change of PBS. For this investigation, the selected stimulus is the mechanical vibration at different frequencies.

The test consists of taking a picture every 10 minutes of a defined geometry of PBS at four different frequencies: 0 Hz, 1 Hz, 5 Hz, 10 Hz using a vibration generator TIRAvib from the company TIRA GmbH (see Figure 4.18). For controlling the desired frequency, it was used a Waveform generator TGA1244 from the company TTi and an analog amplifier BAA 120 from TIRA GmbH (see Figure 4.21). The camera was a Canon EOS 70D equipped with a Macro lens to obtain high-resolution pictures. In addition, the whole test duration per sample had a total duration of 150 minutes and was performed for the PBS1 and PBS2 samples.

Table 4.6.: Shape change test parameters

Parameter	Value
Duration (min)	150
Time lapse (min)	10
Frequencies (Hz)	0, 1, 5, 10
Samples	PBS1 - PBS2

Figure 4.21.: Setup for the shape change test
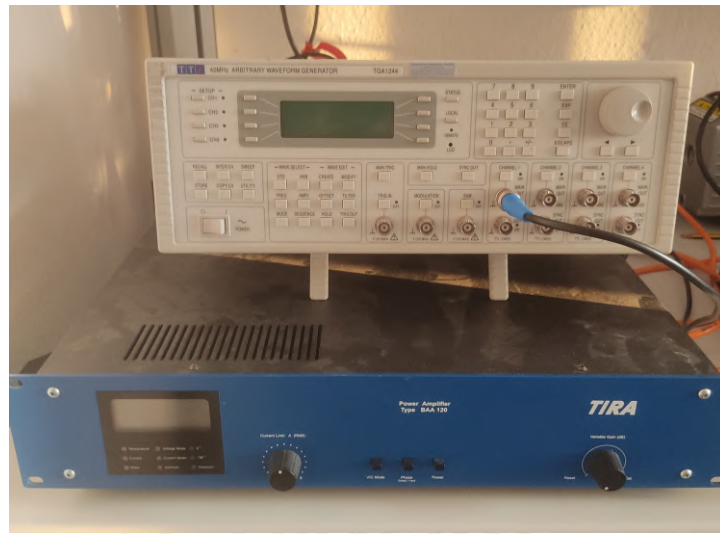
Figure 4.22.: Waveform generator TTi TGA1244 and analog amplifier TIRA BA120

5. Results and Discussion

This chapter presents the result of each characterization test and the discussion of it, comparing it with other investigations. First, this chapter provides the results of the chemical characterization for pure PBS samples and PDMS precursor to find the characteristic chemical bonds that prove the correct synthesis process. Then, it shows the results of the thermogravimetric characterization, which provides the degradation and maximum working temperature of PBS1 and PBS2. Third, it analyzes the rheological characterization for pure PBS and mixed samples to obtain characteristic properties such as linear viscoelastic region (LVER) and gel point. Finally, it presents the change shape test results at different frequencies for PBS1 and PBS2, emphasizing the relation of the chemical structure and deformation capacity.

5.1. Chemical characterization

The results of the FTIR for the PDMS precursors are shown in Figure 5.1. These precursors exhibit $Si(CH_3)_2$ groups at 860 and 1260 cm^{-1}, which experience minimal changes during synthesis. Subsequently, in the range of 1020 to 1090 cm^{-1}, PDMS displays two peaks corresponding to the symmetric vibration of Si-O-Si bonds, and both precursors present CH_3, a type of covalent C-H bond at 2965 cm^{-1}. Finally, in accordance with the investigation conducted by Kurkin et al. [18], PDMS precursors are expected to exhibit a peak at 3700 cm^{-1}, corresponding to non-hydrogen-bonded (free) and intermolecular hydrogen-bonded groups (Si-OH). This comparison of both precursors is illustrated in Figure 5.2, where a peak of OH groups at 3700 cm^{-1} is observed and converted into $B(OH)_x$, providing the viscoelasticity to the PBS. However, in this investigation, PDMS precursors do not exhibit this peak due to the low presence of these groups and the sensitivity limitations of the FTIR test. [49], [67]
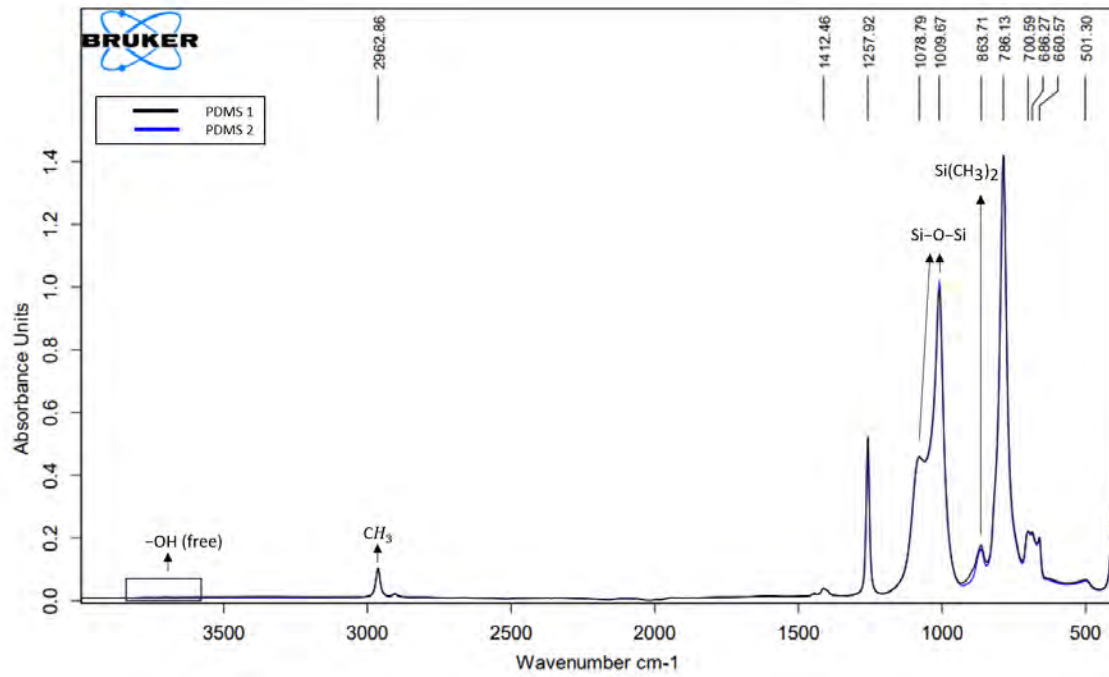
Figure 5.1.: FTIR spectra of PDMS1 and PDMS2 precursors
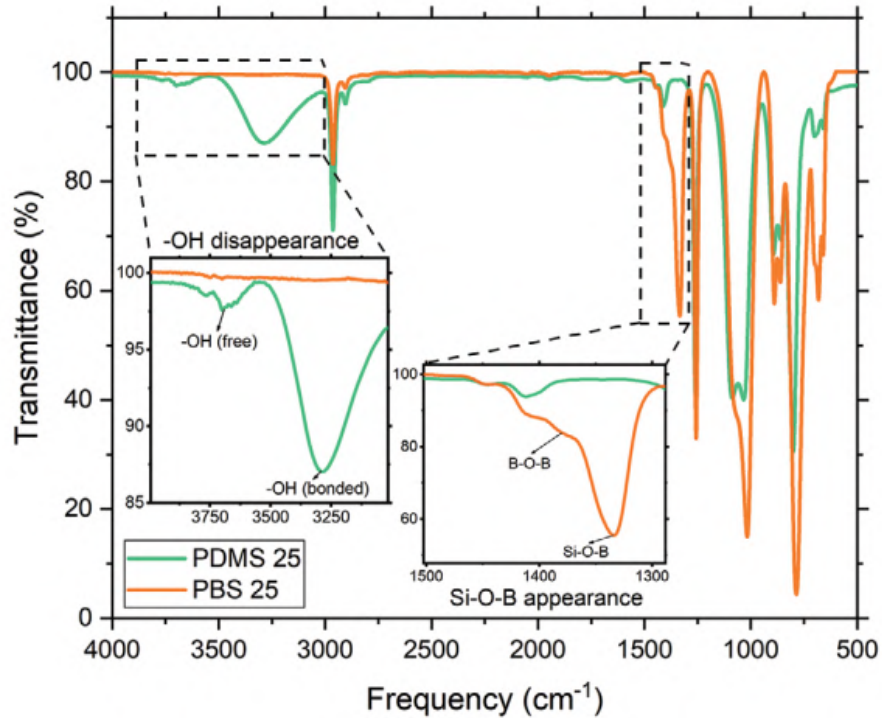
Figure 5.2.: Comparison of FTIR spectra of PBS25 and PDMS25 precursors [18]

The FTIR results of PDMS2, PBS1, and PBS2 are presented in Figure 5.3. These PBS results exhibit the same chemical bonds and groups as PDMS, but they differ significantly at 1340 cm^{-1}, corresponding to the symmetric vibration of Si-O-B bonds. These chemical bonds are responsible for the sticker-like behavior of PBS (rheological behavior) and result from the interaction between boron molecules present in boric acid and hydroxyl groups in the PDMS chains. Additionally, the intensity differences between samples indicate variations in the presence of these bonds in the chemical structure. The PDMS graph is nearly flat because it has not yet reacted with the boric acid. Comparing both PBS samples, PBS1 displays a higher peak than PBS2 due to its shorter molecular chains, allowing for a higher degree of bonding. [18], [49], [6]
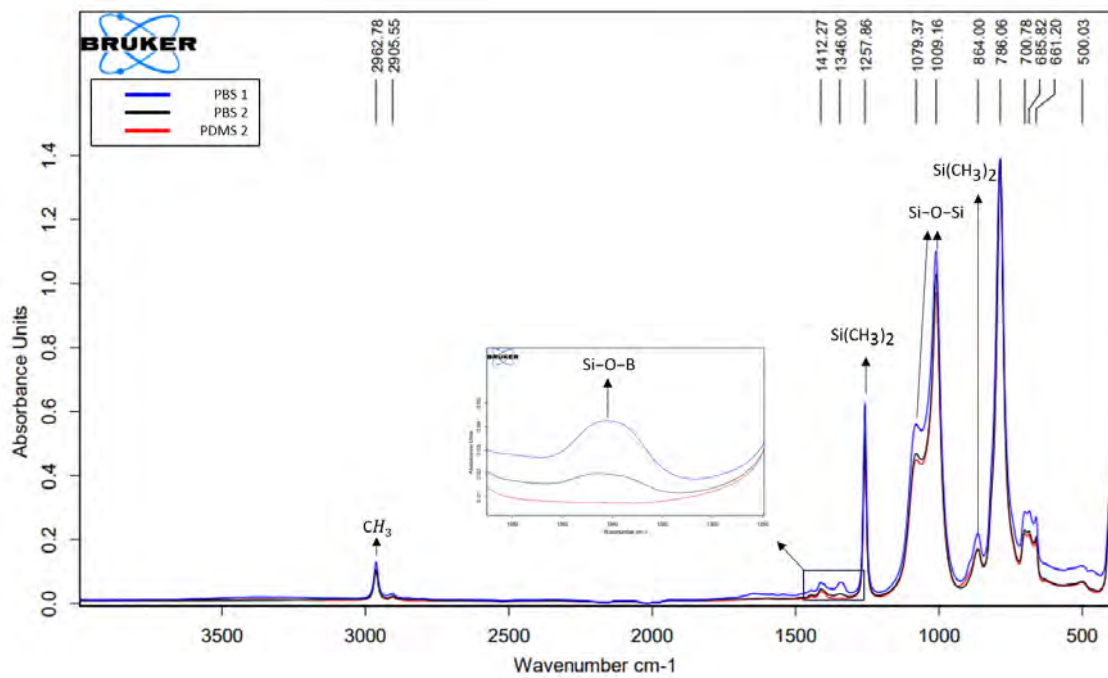
Figure 5.3.: FTIR spectra of PDMS1, PBS1 and PBS2 samples

The Raman spectroscopy results for PBS1 and PBS2 are shown in Figure 5.4. The spectra reveal a peak between 450-550 cm^{-1} corresponding to Si-O-Si bonds and two peaks between 2800-300 cm^{-1} corresponding to CH$_3$ groups. [21] The characteristic dative bonds of PBS appear at 790 cm^{-1}, corresponding to Si-O-B bonds, with a higher peak observed for the PBS1 sample. Additionally, both PBS samples exhibit a peak at 710 cm^{-1} corresponding to B-O-B, indicating the presence of unreacted boric acid. [48], [14]
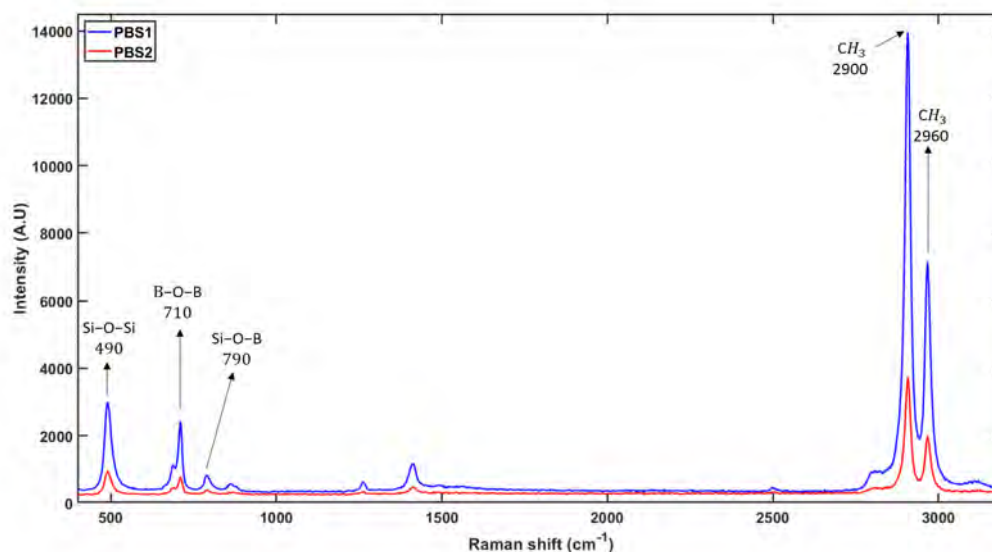
Figure 5.4.: Raman spectra of PBS1 and PBS2 samples

5.2. Morphological characterization

The obtained pictures of the SEM test of the PBS1 are shown in the Figure 5.5. The image on the left side corresponds to the entire sample at 50x magnifications, and the image on the right is an amplification at 2000x magnifications. The last picture shows some traces of boric acid with a maximum size of $13.32\,\mu$m. These traces of boric acid could be from the addition of an excessive precursor or from the high viscosity of the PDMS.

As explained in the previous chapter, the SEM test requires a vacuum inside the device. When it was applied, the samples of PBS1 and PBS2 started to increase in volume due to the difference in pressure of the inside and outside of the samples. This behavior could be due to water molecules or air gaps in the samples.

The results of the stereoscopy test show at better resolution the presence of the non-reacted boric acid with a maximum size of $0.602\,$mm. (See Figure 5.6)
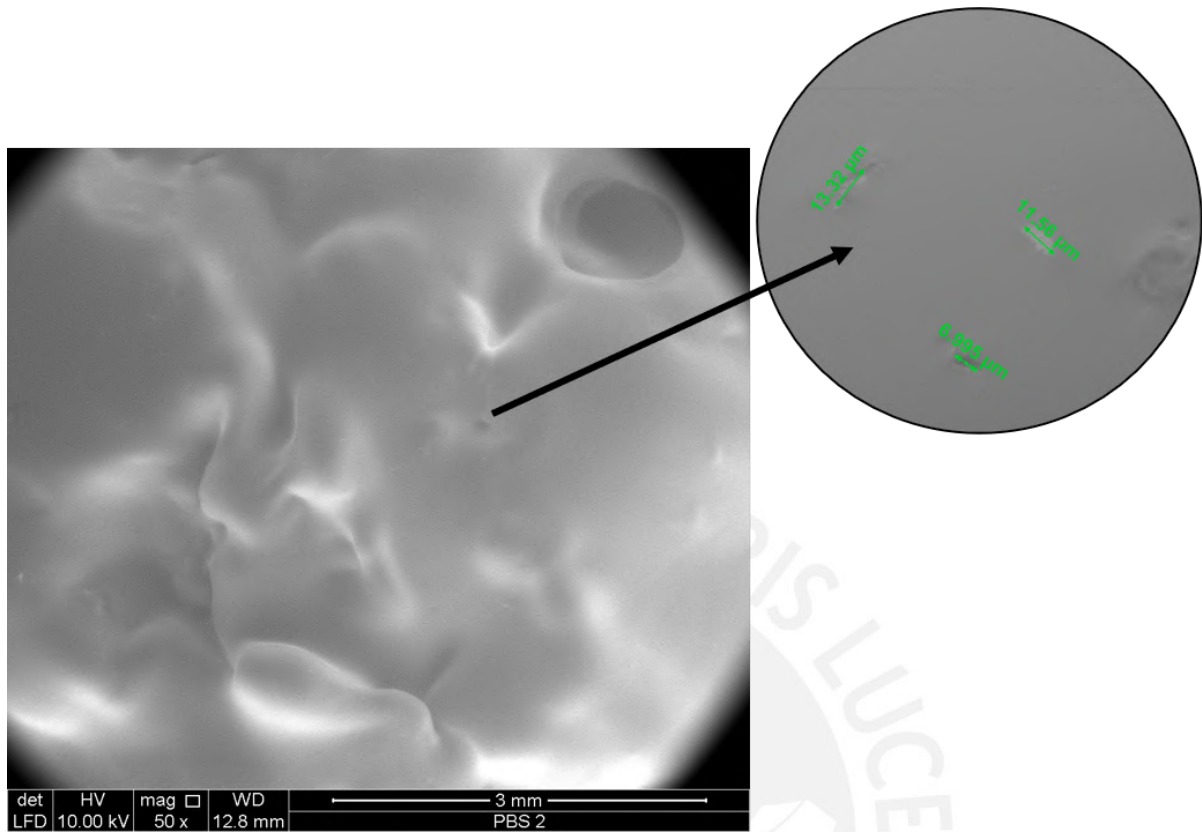
Figure 5.5.: SEM images of the PBS2: At 50x magnifications (left side) and 2000x magnifications (right side)

Figure 5.6.: PBS1 and PBS2 samples during the vacuum process
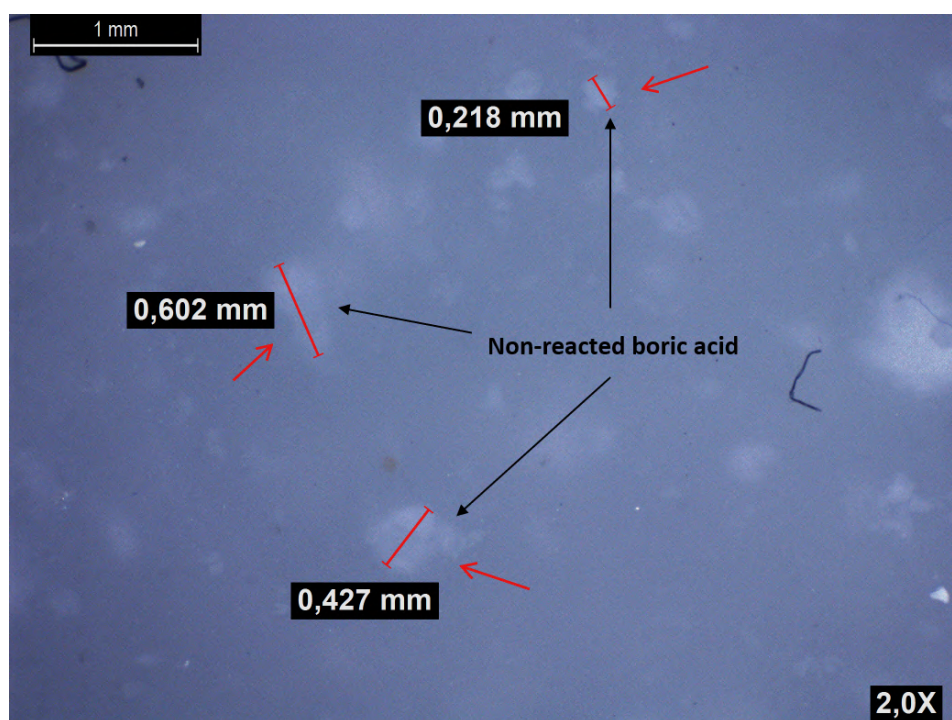
Figure 5.7.: Stereoscopy image of the PBS1 at 2x magnifications

5.3. Termogravimetical characterization

This test was performed for PBS1 and PBS2 to observe the different mass changes at diverse temperatures and obtain the maximum working temperature for the materials. This information will be essential for future investigations and applications of this material. In both result graphics, there are two curves: the red curve corresponds to the mass change of the material, and the green one is the first derivative of this change.

The TGA results for PBS1 and PBS2 are shown in Figure 5.8 and Figure 5.9, respectively. In both curves, the initial weight loss is observed up to $200\,^\circ$C, attributed to absorbed water and the decomposition of methyl groups $Si(CH_3)_2$. The difference in mass change between PBS1 and PBS2 is associated with the varying amounts of absorbed water, with PBS2 exhibiting a higher value. From 250 to $450\,^\circ$C, the second weight loss occurs, linked to the decomposition of organosilicones (Si-O, Si-C, and Si-O-B bonds). Subsequently, at $400\,^\circ$C, the material degradation begins, reaching its maximum rate at $488\,^\circ$C and $422.5\,^\circ$C for PBS1 and PBS2, respectively. The remaining mass for PBS1 is $1.72\,\%$, and for PBS2, it is $1.10\,\%$ of the initial mass, representing the ash content.The summary of the results is presented in Table 5.1. [56]
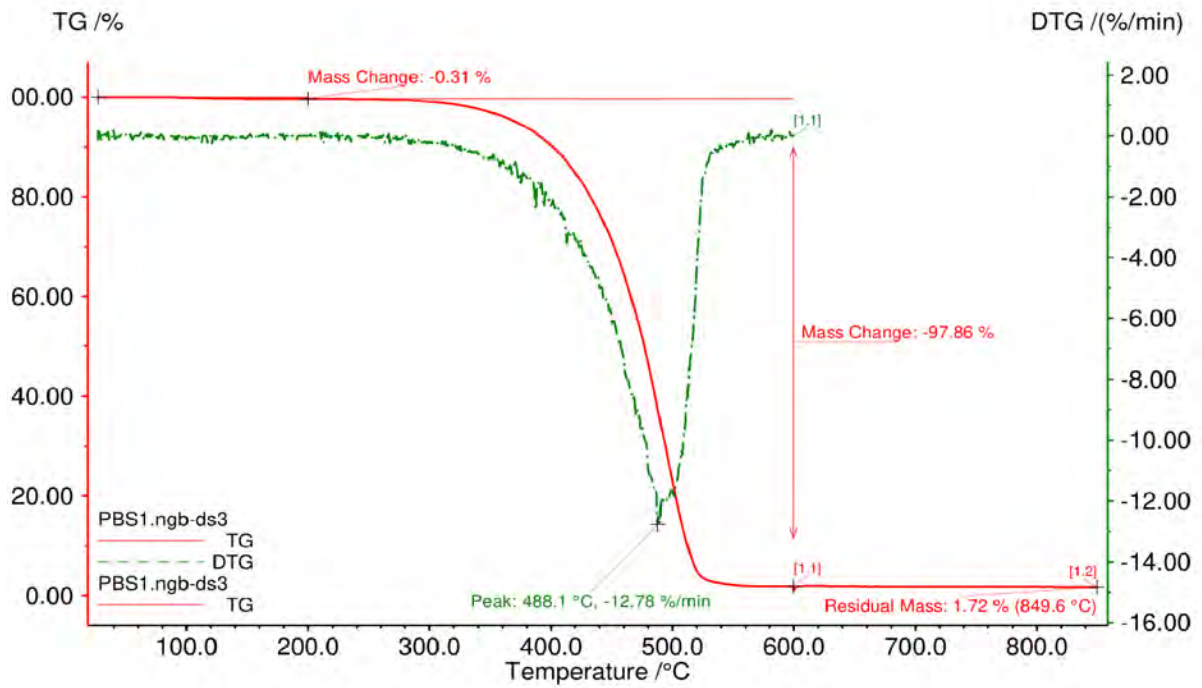
Figure 5.8.: TGA results of the PBS1
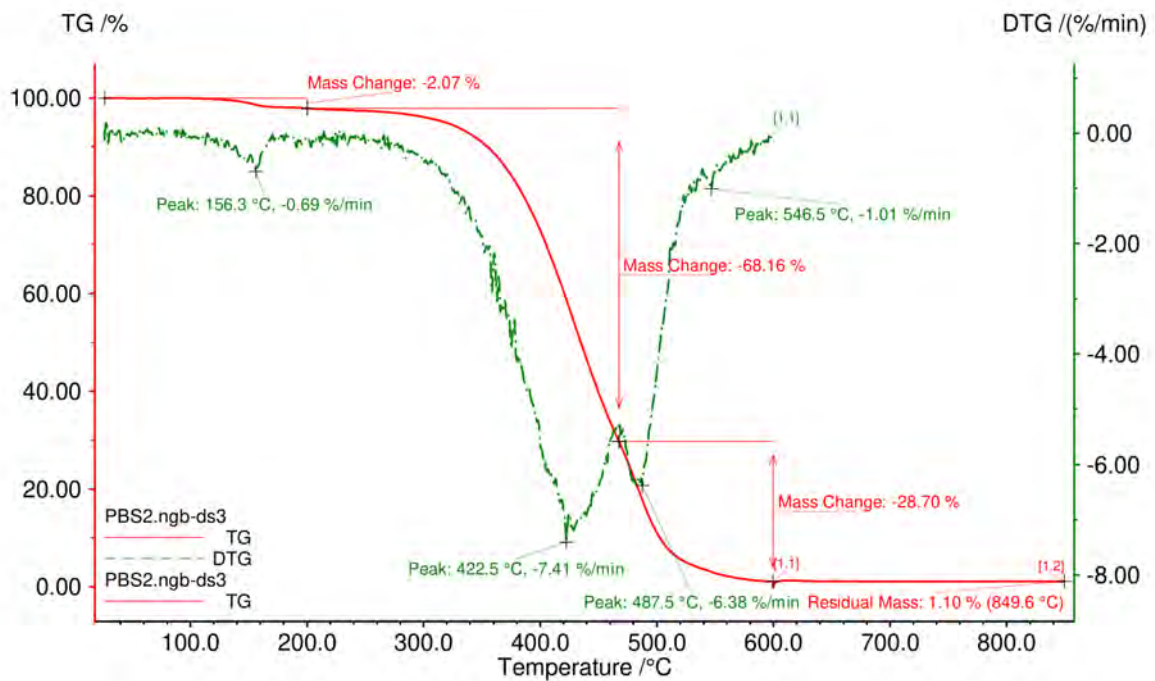
Figure 5.9.: TGA results of the PBS2

Table 5.1.: Start point of degradation and degradation temperature of PBS1 and PBS2

Material	Start of degradation (°C)	Degradation temperature (°C)
PBS1	320	488.1
PBS2	300	422.5

5.4. Rheological characterization

The amplitude sweep test consists into increasing the stress-strain amplitude until the sample's structure degrades (see Figure 5.13), while maintaining a constant oscillation frequency. This test is crucial for identifying the Linear Viscoelastic Region (LVER) of different materials, where the material conserves its structure, characterized by a constant storage modulus over increasing shear strain. In this investigation, the amplitude sweep test provides information of the LVER of PBS, a crucial aspect for the subsequent frequency sweep test, where conserving the PBS structure is necessary.

The results of the amplitude sweep test for all samples are presented in Figure 5.10 and Figure 5.11, summarized in Table 5.2. The end of the LVER was determined by considering a 5 % decrease in the storage modulus. The Y-axis indicates the weight percentage of PBS1 in the mixed PBS. It is evident from the results that the storage modulus of the LVER increases with the percentage of PBS1, and the range of this area expands with the percentage of PBS2. As depicted in Figure 5.12, "Pre-Mixed" PBS samples exhibit a more homogeneous distribution compared to "Post-Mixed" PBS samples, where the data points exhibit higher variability around the trendline. Additionally, for the Post-Mixed samples samples, the influence of the PBS1 begins at 40 %. For percentages below that value, the storage modulus of the LVER exhibits insignificant variability (see Figure 5.11).

Figure 5.10.: Amplitude sweep test result of Pre-Mixed PBS samples. The percentage value represents the percentage in weight of PBS1 in the mixed sample: 0 % represents pure PBS2 and 100 % represents pure PBS1

Figure 5.11.: Amplitude sweep test result of Post-Mixed PBS samples. The percentage value represents the percentage in weight of PBS1 in the mixed sample: 0 % represents pure PBS2 and 100 %represents pure PBS1
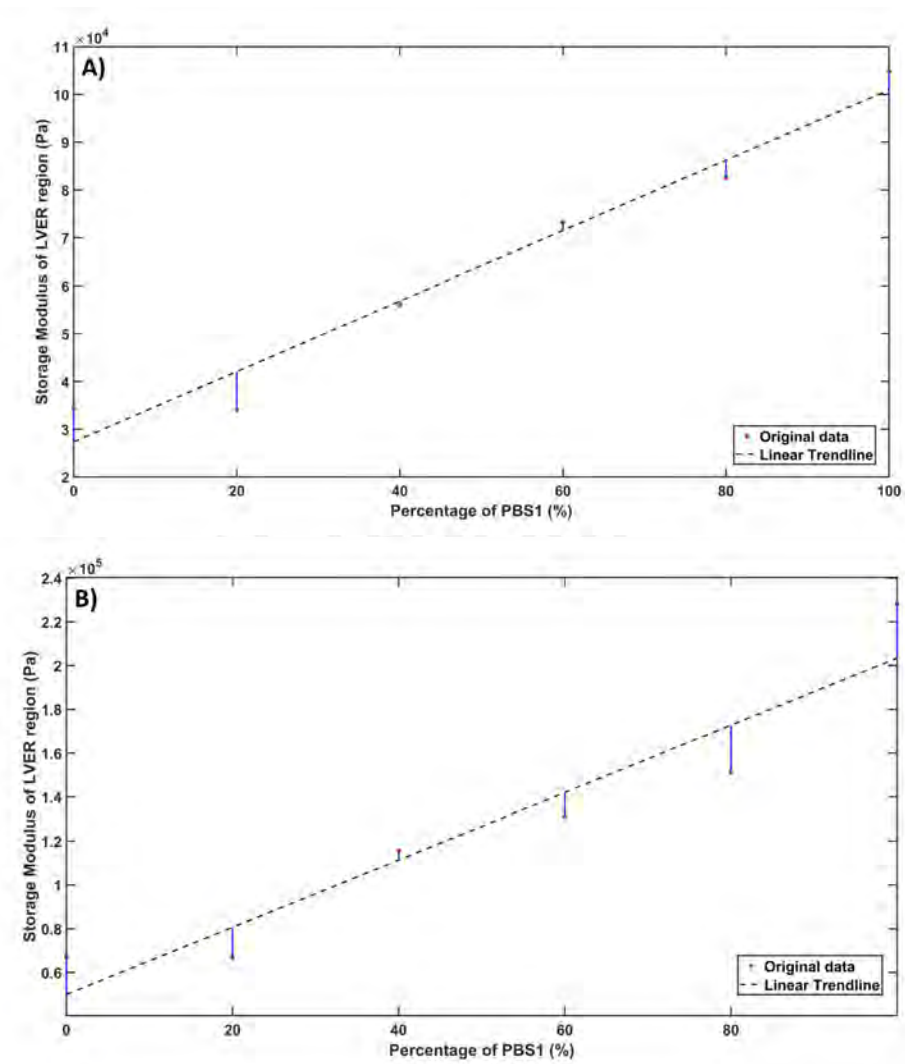
Figure 5.12.: Influence of the percentage of PBS1 on the LVER storage modulus of the mixed PBS: A) Pre-Mixed PBS samples; B) Post-Mixed PBS samples
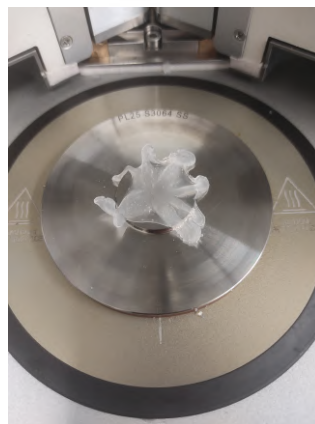
Figure 5.13.: PBS samples after the amplitude sweep test

Table 5.2.: Results of the amplitude sweep test

| | LVER region | | | |
| | Pre-Mixed PBS | | Post-Mixed PBS | |
Samples	Shear (%)	G' (Pa)	Shear (%)	G' (Pa)
PBS1 (100/0)	19.82	228333	19.82	228333
80/20	19.71	184831	25.16	151253
60/40	12.56	127843	25.32	130967
40/60	31.57	112253	31.54	115700
20/80	39.83	87666	40.18	66827
PBS2(0/100)	39.83	67203	39.83	67203

The frequency sweep test graphics for both synthesis processes are presented in Figure 5.14 and Figure 5.15. This test involves increasing the frequency of oscillation while maintaining a constant amplitude. The rise in frequency results in an increasing shear stress rate for PBS, leading to a transition in its behavior from a viscous fluid to a rubbery solid. This transition is known as the gel point and is identified by the intersection of the storage and loss modulus curves. For both PBS samples, the frequency of the gel points is below 0.3 Hz. Furthermore, the inverse of this frequency is referred to as the relaxation time, signifying the time required for the polymer chains to relax and move against each other. The obtained values for all samples align closely with the findings of Tang et al. [49] The summarized properties are presented in Table 5.3.

Additionally, both figures illustrate that the storage modulus G' of the samples increases with the rising frequency. For instance, taking the Post-Mixed PBS sample with 60 % PBS1, at 0.01 Hz, the storage modulus G'*min* registers a value of 94.05 Pa. As the frequency increases, this storage modulus experiences a sudden rise, reaching a value of $112 \cdot 10^3$ Pa G'*max* at 100 Hz. This increase in storage modulus aligns with the shear stiffening effect of PBS. At low frequencies (low shear stress rate), the molecular chains have sufficient time to relax and reconnect, allowing chain movement. However, at high frequencies (high shear stress rate), the molecular chains lock, increasing stiffness. To assess this effect in different PBS samples, Wang et al. [56] defined a relative shear stiffening effect (RSTe) (see equation 5.1), which considers the values of G'*min* and G'*max*. The summarized properties are provided in Table 5.4.

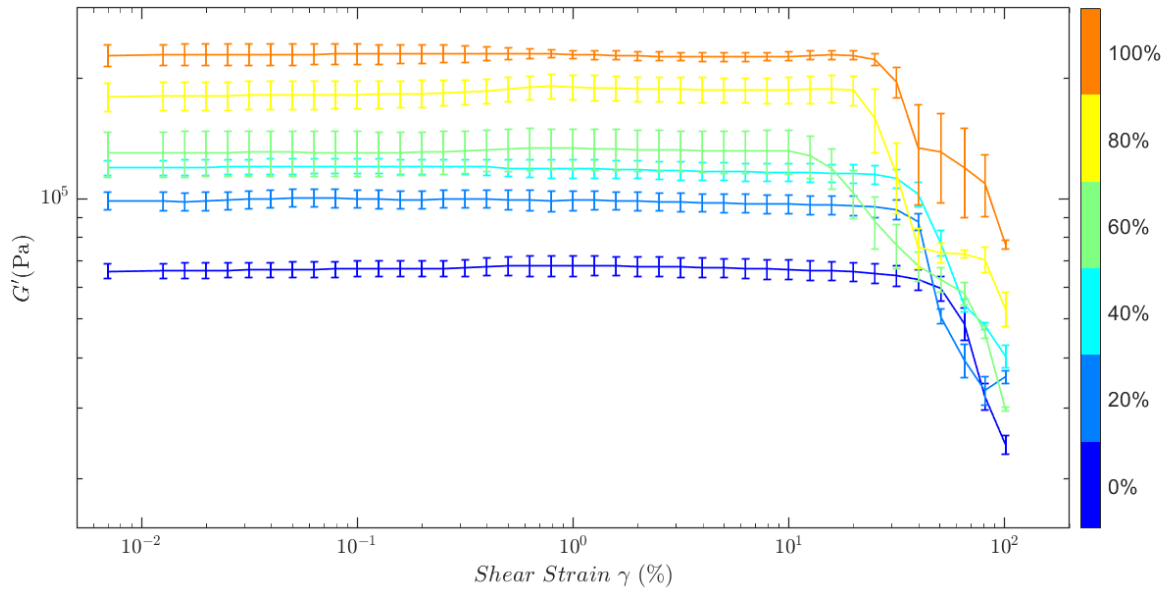$$RSTe(\%) = \frac{G'_{\text{max}} + G'_{\text{min}}}{G'_{\text{min}}} \times 100 \tag{5.1}$$
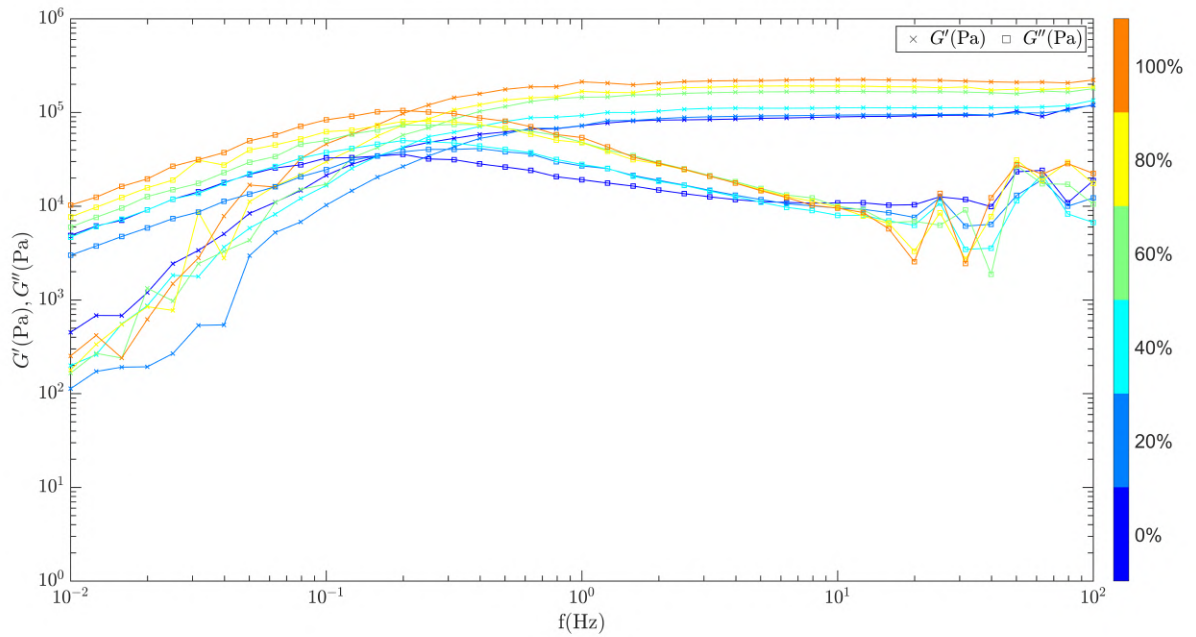
Figure 5.14.: Frequency sweep test result of Pre-Mixed PBS samples. The percentage value represents the percentage in weight of PBS1 in the mixed sample: 0% represents pure PBS2 and 100% represents pure PBS1
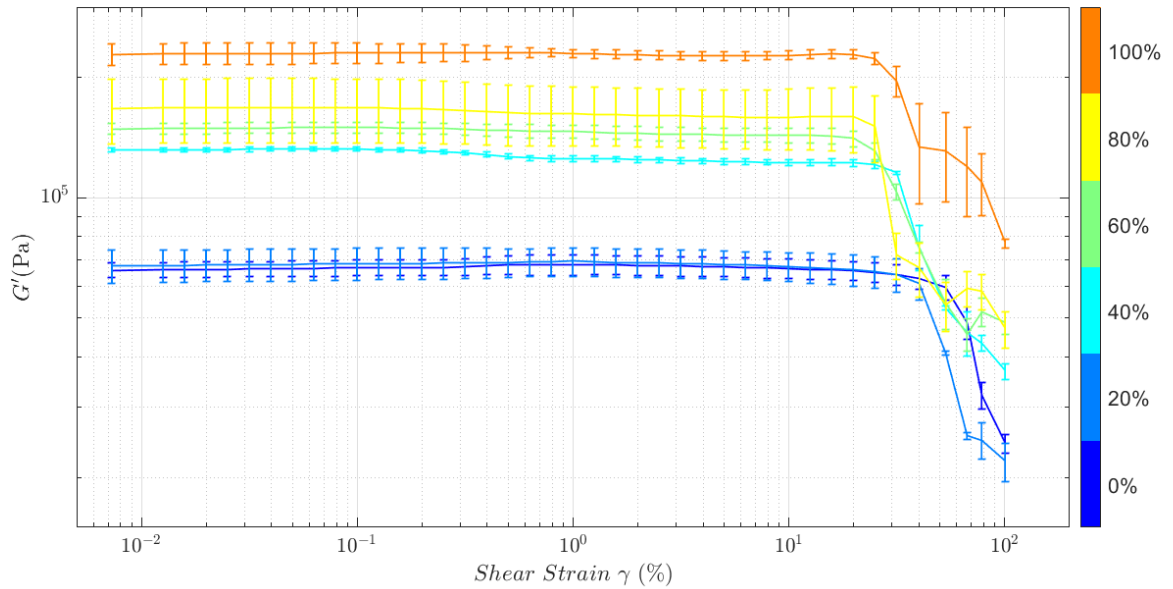

Figure 5.15.: Frequency sweep test result of Post-Mixed PBS samples. The percentage value represents the percentage in weight of PBS1 in the mixed sample: 0% represents pure PBS2 and 100% represents pure PBS1
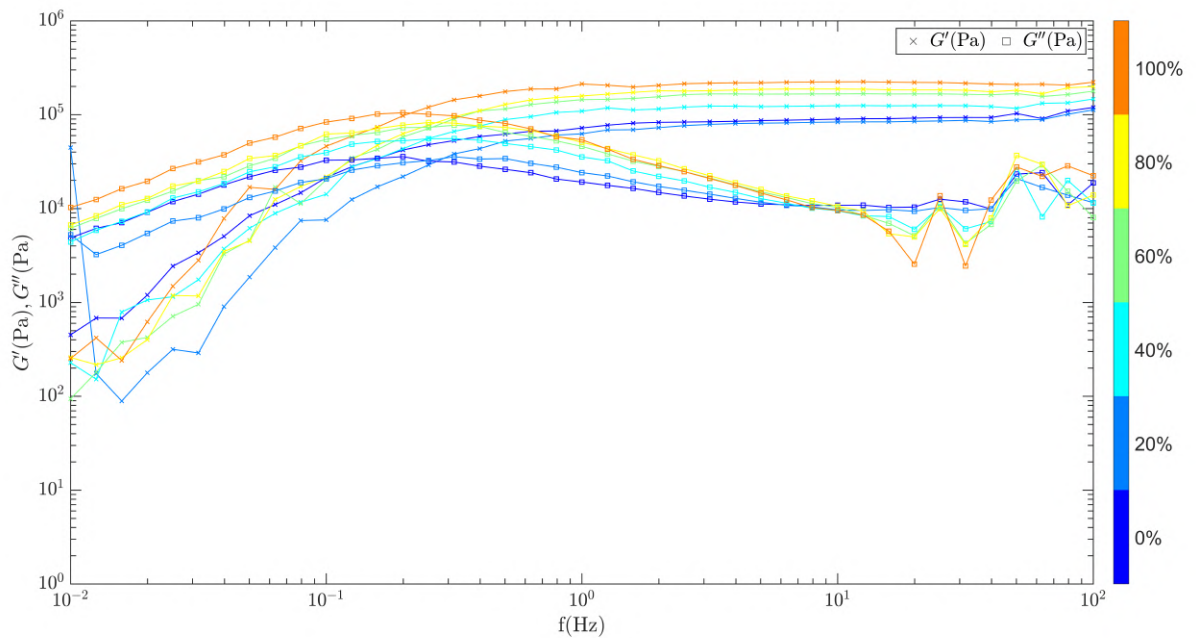
Table 5.3.: Results of the frequency sweep test

	Gel Point					
	Pre-Mixed PBS			**Post-Mixed PBS**		
Samples	Frequency (Hz)	Relaxation time (s)	G' (Pa)	Frequency (Hz)	Relaxation time (s)	G' (Pa)
PBS1 (100/0	0.20	0.80	104867	0.20	0.80	104867
80/20	0.26	0.60	82530	0.23	0.71	80602
60/40	0.25	0.63	73243	0.25	0.63	73010
40/60	0.25	0.63	55910	0.23	0.71	49520
20/80	0.28	0.56	34056	0.32	0.50	40383
PBS2(0/100)	0.16	1.00	34377	0.16	1.00	34377

Table 5.4.: Summary of Relative shear stiffening effect (RSTe) values

	Relative shear stiffening effect (RSTe)					
	Pre-Mixed PBS			**Post-Mixed PBS**		
Samples	G'_{max}	G'_{min}	RSTe (%)	G'_{max}	G'_{min}	RSTe (%)
PBS1 (100/0)	$4.52 \cdot 10^2$	$1.19 \cdot 10^5$	26 305.020 21	$4.52 \cdot 10^2$	$1.19 \cdot 10^5$	26 305.0202
80/20	$1.13 \cdot 10^2$	$1.21 \cdot 10^5$	107 108.7205	$1.80 \cdot 10^2$	$1.13 \cdot 10^5$	62 455.4698
60/40	$2.00 \cdot 10^2$	$1.35 \cdot 10^5$	67 401.251 88	$2.28 \cdot 10^2$	$1.47 \cdot 10^5$	64 325.3662
40/60	$1.66 \cdot 10^2$	$1.80 \cdot 10^5$	107 900.8181	$9.41 \cdot 10^1$	$1.78 \cdot 10^5$	189 054.705
20/80	$1.78 \cdot 10^2$	$1.87 \cdot 10^5$	104 841.0444	$2.60 \cdot 10^2$	$1.99 \cdot 10^5$	76 717.5916
PBS2(0/100)	$2.53 \cdot 10^2$	$2.22 \cdot 10^5$	87 722.862 18	$2.53 \cdot 10^2$	$2.22 \cdot 10^5$	87 722.8622

5.5. Shape change test

The obtained images of the shape change test for each frequency were processed using the software ImageJ®. This software has different tools to measure defined or irregular shapes and provide parameters such as the samples' area, perimeter, or minimum and maximum radius. In the shape change test, the tool "oval" is used to provide a reliable approximation to the defined geometry of the PBS. In addition, the selection of the oval was done manually to reduce the error because the sample has residual material in its boundary that might affect the selection of it using a filter. The following procedure is shown in the next steps and is represented in Figure 5.17.

1. select "Analyze" and " Set scale" to define a scale. In this case, three graph paper squares were selected, corresponding to 3 millimeters;

2. select "Analyze" and enable in "Set measurements" the "min & max gray value" to obtain the maximum and minimum radius of the samples and its average;

3. use the "Oval" shape and fit it to the edges of the PBS sample;

4. select "Analyze" and "Measure" to obtain the sample measures.

The start diameter of each sample according to the mold is 15 millimeters, but this value varied at the start of the test because of the manual molding and trimming process (from 14.8 to 15.2 mm). For that reason, the percentage of deformation is calculated considering the initial average diameter and the average diameter for each point. The following equation is shown in Equation 5.2.

$$\text{Deformation } (\%) = \frac{\text{Diameter} - \text{Diameter}_0}{\text{Diameter}_0} \times 100 \tag{5.2}$$

The results for both PBS samples are presented in Figure 5.17 and Figure 5.18, with a summary in Table 5.5. In the case of PBS1, the lowest shape change occurred at 1 Hz, while the highest was at 0 Hz (No stimuli). Furthermore, the maximum deformation after 150 minutes was 15.5 %, observed at 0 Hz. For PBS2, the lowest shape change rate was observed at 1 Hz, with the highest at 5 Hz. The maximum deformation of this sample after the test was 27.8 % at 5 Hz.

Comparing both sets of results, it is evident that PBS1 exhibits a lower final deformation percentage, with its four curves closer than PBS2. This observation suggests that different frequency vibrations have a lesser influence on the shape retainability for PBS1 than PBS2. This difference is attributed to the higher number of dynamic bonds in PBS1, which are also associated with the PDMS precursor. When a frequency above the gel point is applied, these bonds act as crosslinking points, restricting chain movement and reducing the deformation rate. These insights provide important information of the behavior of PBS under vibrational stimuli at frequencies up to the gel point, leading to the conclusion that a lower viscosity PDMS precursor enhances the shape retainability of PBS at different frequencies.
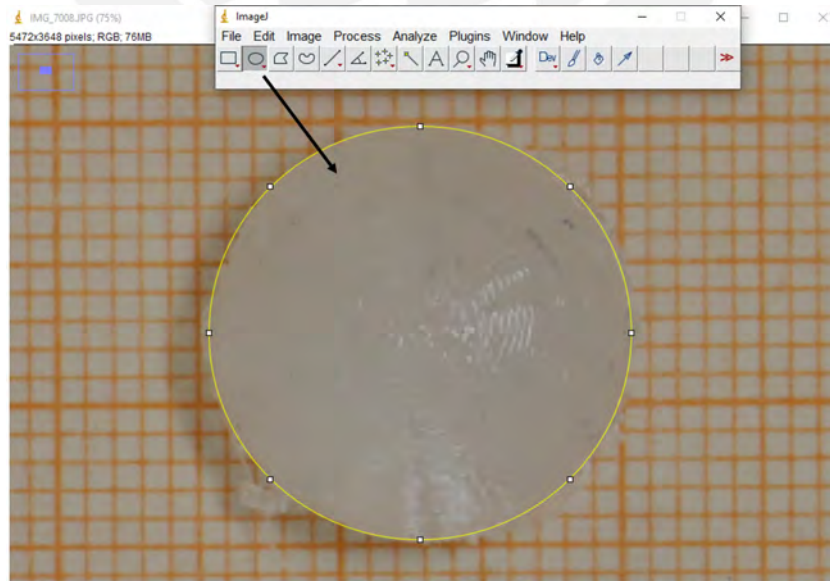
Figure 5.16.: Processing procedure of the obtained images through ImageJ® software
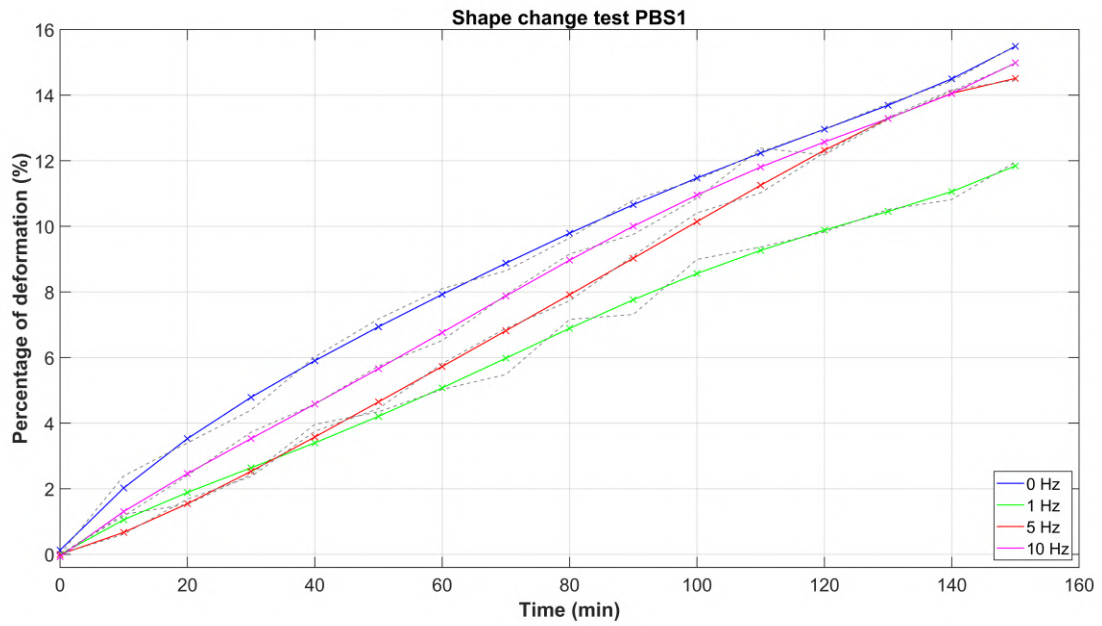
Figure 5.17.: Percentage of deformation in PBS1 over time at four different frequencies
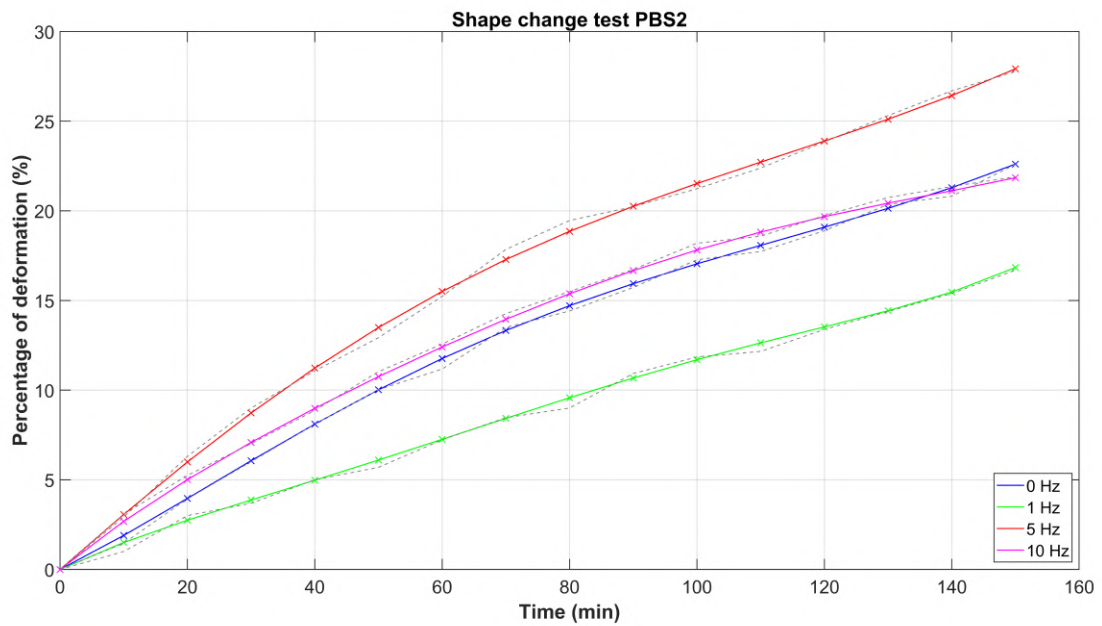
Figure 5.18.: Percentage of deformation in PBS2 over time at four different frequencies

Table 5.5.: Summary of results from the shape change test

	PBS 1				PBS2			
Time (min)	0 Hz	1 Hz	5 Hz	10 Hz	0 Hz	1 Hz	5 Hz	10 Hz
0	0.0	0.0	0.0	0.0	0.0	0.0	0.0	0.0
10	2.4	1.2	0.6	1.2	1.5	1.0	2.9	3.1
20	3.4	1.5	1.7	2.4	3.9	3.0	6.3	5.2
30	4.4	2.4	2.4	3.7	6.0	3.7	9.0	7.0
40	6.0	4.0	3.8	4.6	8.1	5.0	11.1	8.9
50	7.2	4.3	4.4	5.7	10.0	5.7	12.9	11.0
60	8.1	5.0	5.8	6.5	11.2	7.2	15.2	12.6
70	8.6	5.5	6.9	7.9	13.5	8.5	17.8	14.3
80	9.6	7.2	7.7	9.2	14.4	9.0	19.5	15.5
90	10.8	7.3	9.1	9.8	15.7	10.9	20.2	16.7
100	11.4	9.0	10.4	10.9	17.3	11.8	21.2	18.2
110	12.3	9.4	11.0	12.4	17.7	12.2	22.4	18.6
120	13.0	9.8	12.2	12.2	18.9	13.4	23.8	19.7
130	13.7	10.5	13.3	13.3	20.4	14.4	25.3	20.7
140	14.4	10.8	14.2	14.1	20.8	15.4	26.7	21.4
150	15.5	12.0	14.5	15.0	22.6	16.7	27.8	21.9

Percentage of deformation (%) at different frequencies
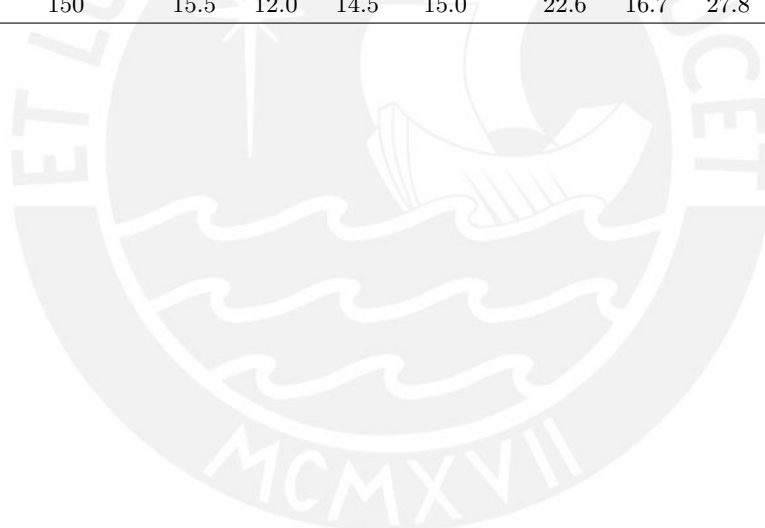
6. Conclusions and Outlook

6.1. Conclusions

Initially, polyborosiloxane samples were produced using polydimethylsiloxanes with two distinct viscosities, one higher than the other. These samples were categorized into three groups: Pure PBS samples, formed by combining the two PDMS precursors; Pre-mixed PBS samples, created by blending the two PDMS precursors in different weight ratios; and Post-mixed PBS samples, generated by mixing the two pure PBS samples in the same ratios as the second category. Chemical and morphological characterizations were conducted to identify the various chemical bonds present in the samples and compare them with findings from other studies. Additionally, the three categories were tested by amplitude and frequency sweep tests to evaluate the influence of the mixing procedure and precursors on their rheological properties. Finally, a shape change test at different frequencies was performed to assess the impact of mechanical stimuli (vibrations) on their shape retainability.

From the chemical characterization tests, it can be concluded that the synthesized materials correspond to polyborosiloxane, as the samples exhibit the characteristic Si-O-B bonds. These bonds contribute to the unique viscoelastic behavior of this material, resulting from the interaction between the PDMS hydroxyl groups (OH) and boron atoms of Boric Acid. Furthermore, the differences in peak intensities of Si-O-B confirm the influence of precursor viscosity on the number of dative bonds. Raman Spectroscopy reveals peaks related to B-O-B groups, indicating the presence of non-reacted boric acid. This result is corroborated by morphological characterization, where traces of unreacted boric acid are observed on the PBS surface.

In the amplitude sweep test, it is concluded that the intensity of Si-O-B bonds influences the storage modulus within the LVER, with the highest storage modulus obtained at $100\,\%$ of PBS1. Additionally, comparing the results of Pre-mixed samples and Post-mixed samples, it is concluded that Pre-mixed samples exhibit a more homogeneous distribution compared to Post-mixed samples. These results suggest that the Pre-mixed method allows for a better prediction of rheological properties for different mixing ratios. Moreover, in samples fabricated after synthesis, the addition of PBS1 begins to influence its rheological properties up to $40\,\%$ of this material. In the frequency sweep test, it is concluded that PBS exhibits a significant shear stiffening effect, reaching a maximum value of $1.89 \cdot 10^5\,\%$, corresponding to mixed PBS with a content of $60\,\%$ in mass of PBS1. Also, the calculated frequency and relaxation time for all samples are below $0.3\,\mathrm{Hz}$ and $1\,\mathrm{s}$, respectively. These values provide information about the frequency at which PBS shifts from a viscous liquid to a solid rubbery state, crucial for its application in soft robotics.

Analysis of the shape change graphs for PBS1 and PBS2 samples indicated that mechanical stimuli (vibration) affected the shape retention capacity with variations between the two samples. For PBS1, the highest deformation occurred at 0 Hz, while the lowest was at 1 Hz. This PBS sample exhibited lower deformation at each frequency than in the absence of stimuli, attributed to the relaxation behavior of dynamic bonds. In contrast, PBS2 showed different frequencies for the highest and lowest deformation (5 Hz and 1 Hz, respectively) and demonstrated higher deformation than PBS1 at each frequency, linked to the number of chemical bonds present in both samples.

6.2. Outlook

In this study, the established synthesis process resulted in PBS samples featuring characteristic Si-O-B bonds, which provides the unique viscoelasticity of the material. However, the presence of unreacted boric acid moieties in the structure was also observed, potentially impacting the properties of these samples. To solve this issue, incorporating a purification step after the synthesis process is recommended. This purification step involves dissolving the PBS in Hexane and filtering it [21]. Additionally, after the fabrication of PBS, these samples initially exhibited brittle behavior, contrary to findings in some previous investigations [18], [49]. Over three days, the PBS behavior transitioned to a softer state due to water absorption from the environment, forming $Si-O-B(OH)_2$ groups and adding viscoelasticity. To manage this behavior change, evaluating PBS water absorption over time and determining its maximum water absorption would be beneficial.

Temperature has been identified as a factor influencing the rheological properties of PBS, as explored by Golinelli et al., although exclusively for pure PBS samples [11]. Therefore, future investigations could investigate into the temperature's impact on the rheological properties, including gel point, relaxation time, storage modulus, and loss modulus, for both Pre-mixed and Post-mixed samples.

The results of the shape change test indicate that mechanical stimuli (vibrations) influence the shape retainability of the evaluated material. To gain deeper insights into this influence, future investigations could assess PBS samples at frequencies close to the gel point. These findings would reveal the optimal vibration frequency at which PBS transitions from a viscous fluid to a solid, considering different mixing ratios. Additionally, enhancing this retainability could involve adding different fillers such as iron nanoparticles or thermoplastics with a low fusion point. The outcomes of such investigations would provide crucial information for the application of PBS in soft robotics and other mechanical systems. The results from this investigation would provide important information for PBS application in soft robotics and other mechanical systems.

Bibliography

[1] ABCR: AB111937 | CAS 70131-67-8. 2023. URL: https://abcr.com/de_en/ab111937.

[2] ANTON PAAR: Amplitude Sweeps. 2022. URL: https://wiki.anton-paar.com/ca-en/amplitude-sweeps/.

[3] BAHL, S.; NAGAR, H.; SINGH, I., and SEHGAL, S.: Smart materials types, properties and applications: A review. In: Materials Today: Proceedings 28 (2020). DOI: 10.1016/j.matpr.2020.04.505.

[4] BERTHOMIEU, C. and HIENERWADEL, R.: Fourier transform infrared (FTIR) spectroscopy. In: Photosynthesis research 101 (2009). DOI: 10.22214/ijraset.2022.40147.

[5] BONTEN, C.: 3 - Plastics Materials Engineering. In: (2019). DOI: https://doi.org/10.3139/9781569907689.003.

[6] CHANG, Z.: A Multifunctional Silly-Putty Nanocomposite Spontaneously Repairs Cathode Composite for Advanced LiS Batteries. In: Advanced Functional Materials 28 (December 2018). DOI: 10.1002/adfm.201804777.

[7] COASEY, K.: Section I: Rheology (DMA) Theory, Instrumentation, and basic methods. 2022. URL: https://www.tainstruments.com/wp-content/uploads/8-29-22-Rheology-Presentation-part-1-SJ.pdf.

[8] DROZDOV, F. V.; MANOKHINA, E. A.; VU, T. D., and MUZAFAROV, A. M.: Polyborosiloxanes (PBS): Evolution of Approaches to the Synthesis and the Prospects of Their Application. In: Polymers (2022). DOI: 10.3390/polym14224824.

[9] GATEWAY ANALYTICAL: Comparison of Raman and FTIR Spectroscopy: Advantages and Limitations. 2023. URL: https://gatewayanalytical.com/comparison-of-raman-and-ftir-spectroscopy-advantages-and-limitations/.

[10] GENCER, A. and OKSAL, B. S.: Synthesis and characterization of novel SiBOC ceramics: comparison of microwave and ultrasonic application on gelation time. In: Sol-Gel Science and Technology (2015). DOI: 10.1007/s10971-014-3508-0.

[11] GOLINELLI N Spaggiari A, D. E.: Mechanical behaviour of magnetic Silly Putty: Viscoelastic and magnetorheological properties. Journal of Intelligent Material Systems and Structures. In: Intelligent Material Systems and Structures (2017). DOI: 10.1177/1045389X15591655.

[12] GREISINGER: GTH 175 PT. 2023. URL: https://www.greisinger.de/files/upload/en/produkte/bda/GTH175_PT_EN.pdf.

[13] HARTMANN, L.; REICH, R.; KLETZIN, U., and ZENTNER, L.: Approaches on material analysis and modeling of bouncing putty. In: (2014).

[14] HE, F.; HE, Z.; XIE, J., and LI, Y.: IR and Raman Spectra Properties of Bi_2O_3-ZnO-B_2O_3-BaO Quaternary Glass System. In: American Journal of Analytical Chemistry (2014). DOI: 10.4236/ajac.2014.516121.

[15] JUHASZ, A.; TASNADI, P., and FABRY, L.: Impact studies on the mechanical properties of polyborosiloxane. In: Physics Education 19.6 (1984), pp. 302–304. DOI: 10.1088/00 31-9120/19/6/315.

[16] JULABO: CF41 Cryo-compact circulator. 2023. URL: https://www.julabo.com/en-gb /products/refrigerated-circulators/cryo-compact-circulators/cf41.

[17] KULKARNI, V. S. and SHAW, C.: Chapter 9 - Rheological Studies. 2016. ISBN: 978-0-12-801024-2. DOI: https://doi.org/10.1016/B978-0-12-801024-2.00009-1.

[18] KURKIN, A.; LIPIK, V.; TAN, K. B. L.; SEAH, G. L.; ZHANG, X., and TOK, A. L. Y.: Correlations Between Precursor Molecular Weight and Dynamic Mechanical Properties of Polyborosiloxane (PBS). In: Macromolecular Materials and Engineering (2021). DOI: 10.1002/mame.202100360.

[19] LI, M.; PAL, A.; BYUN, J.; GARDI, G., and SITTI, M.: Magnetic Putty as a Reconfigurable, Recyclable, and Accessible Soft Robotic Material. In: Advanced Materials (2023). DOI: https://doi.org/10.1002/adma.202304825.

[20] LIANG, J. and ZHANG, X.-H.: Rheological Properties of SP in Shock Transmission Application. In: Journal of Materials in Civil Engineering (2014). DOI: 10.1061/(ASC E)MT.1943-5533.0001227.

[21] LIU, B. and FU, J.: Modulating surface stiffness of polydimethylsiloxane (PDMS) with kiloelectronvolt ion patterning. In: Journal of Micromechanics and Microengineering (2015). DOI: 10.1088/0960-1317/25/6/065006.

[22] MAHAPATRA, S. D.; MOHAPATRA, P. C.; ARIA, A. I.; CHRISTIE, G.; MISHRA, Y. K.; HOFMANN, S., and THAKUR, V. K.: Piezoelectric Materials for Energy Harvesting and Sensing Applications: Roadmap for Future Smart Materials. In: Advanced Science 8.17 (2021). DOI: https://doi.org/10.1002/advs.202100864.

[23] MALVERN INSTRUMENTS: A Basic Introduction to Rheology. 2016. URL: https://cdn .technologynetworks.com/TN/Resources/PDF/WP160620BasicIntroRheology.pdf.

[24] NABAVI, S. F.; FARSHIDIANFAR, A., and AFSHARFARD, A.: Novel piezoelectric-based ocean wave energy harvesting from offshore buoys. In: Applied Ocean Research 76 (2018), pp. 174–183. ISSN: 0141-1187. DOI: https://doi.org/10.1016/j.apor.2018.05.00 5.

[25] NANOSCIENCE INSTRUMENTS: Scanning Electron Microscopy. 2023. URL: https://w ww.nanoscience.com/techniques/scanning-electron-microscopy/.

[26] NETZSCH: Linear Viscoelastic Region (LVER). 2022. URL: https://analyzing-testing.netzsch.com/en/training-know-how/glossary/linear-viscoelastic-region-lver.

[27] NETZSCH: Kinexus pro+. 2023. URL: https://analyzing-testing.netzsch.com/es/productos/reologia/modular-rheometers-for-all-applications/kinexus-pro.

[28] NETZSCH: STA 449 F1 Jupiter. 2023. URL: https://analyzing-testing.netzsch.com/es/productos/termogravimetria-simultanea-calorimetria-de-barrido-diferencial/sta-449-f1-jupiter.

[29] OHAUS: GUARDIAN 3000. 2023. URL: https://eu-de.ohaus.com/de-eu/guardian3000-13.

[30] PERKIN LMER: Thermogravimetric Analysis (TGA)-A Beginner's Guide. 2023. URL: https://resources.perkinelmer.com/lab-solutions/resources/docs/faq_beginners-guide-to-thermogravimetric-analysis_009380c_01.pdf.

[31] PURDUE UNIVERSITY: Scanning Electron Microscope. 2023. URL: https://www.purdue.edu/ehps/rem/laboratory/equipment%20safety/Research%20Equipment/sem.html.

[32] QADER, I.; KÖK, M.; DAGDELEN, F., and AYDOGDU, Y. F.: A Review of Smart Materials: Researches and Applications. In: El-Cezerî Journal of Science and Engineering (2019). DOI: 10.31202/ecjse.562177.

[33] RAMIREZ, D. and VILCA, M.: Rheological properties of polyborosiloxane (PBS) and its application in tensegrity structure [Unpublished manuscript]. In: (2023).

[34] RAMLI, H.; ZAINAL, N. F. A.; HESS, M., and CHAN, C. H.: Basic principle and good practices of rheology for polymers for teachers and beginners. In: Chemistry Teacher International (2022). DOI: 10.1515/cti-2022-0010.

[35] RENISHAW: inVia™ confocal Raman microscope. 2023. URL: https://www.renishaw.com/en/invia-confocal-raman-microscope--6260.

[36] REUSS, J.: Untersuchungen zu den herstellungsbezogenen und rheologischen Eigenschaften von Borsilikonkitt [Master thesis]. In: (2016).

[37] RHEOLOGY TESTING SERVICE: Frequency Sweep. 2017. URL: https://www.rheologytestingservices.com/frequency-sweep.

[38] RICHARDSON, S. M.: Non-Newtonian Fluids. In: (2011). DOI: 10.1615/AtoZ.n.non-newtonian_fluids.

[39] ROHMAN, A.; WINDARSIH, A.; LUKITANINGSIH, E.; RAFI, M.; BETANIA, K., and FADZILLAH, N. A.: The use of FTIR and Raman spectroscopy in combination with chemometrics for analysis of biomolecules in biomedical fluids: A review. In: Biomedical Spectroscopy and Imaging 8.3-4 (2019), pp. 55–71. DOI: 10.3233/BSI-200189.

[40] SCHRODER, T.: Rheologie der Kunststoffe. 2018. ISBN: 978-3-446-45405-7.

[41] Seetapan, N.; Fuongfuchat, A.; Sirikittikul, D., and Limparyoon, N.: Unimodal and bimodal networks of physically crosslinked polyborodimethylsiloxane: Viscoelastic and equibiaxial extension behaviors. In: Journal of Polymer Research 20 (July 2013). doi: 10.1007/s10965-013-0183-8.

[42] SHIMADZU: FTIR Attenuaded Total Reflectance (ATR. 2023. url: https://www.ssi.shimadzu.com/products/ftir/ftir-spectroscopy-consumables/attenuated-total-reflectance/index.html.

[43] Shukla, U. and Garg, K.: Journey of smart material from composite to shape memory alloy (SMA), characterization and their applications-A review. In: Smart Materials in Medicine 4 (2023), pp. 227–242. issn: 2590-1834. doi: https://doi.org/10.1016/j.smaim.2022.10.002.

[44] Sigma Aldrich: Boric acid. 2023. url: https://www.sigmaaldrich.com/DE/en/product/sigma/b6768?gclid=EAIaIQobChMIzKa_-_yA_wIVEtJ3Ch0wwgh5EAAYASAAEgIOCPD_BwE&gclsrc=aw.ds.

[45] Sigma Aldrich: Poly(dimethylsiloxane), hydroxy terminated. 2023. url: https://www.sigmaaldrich.com/DE/es/product/aldrich/481963.

[46] Spectra Lab: Bruker Tensor 27 FT-IR Spectrometer. 2023. url: https://spectralabsci.com/equipment/bruker-tensor-27-ft-ir-spectrometer/.

[47] TA Instruments: Thermogravimetric Analysis (TGA)-Theory and Applications. 2023. url: https://www.tainstruments.com/wp-content/uploads/San-Jose-Thermal-TGA.pdf.

[48] Tamayo, A.; Pérez-Villar, S.; Rubio, F.; Rodríguez, M.; Rubio, J., and Oteo, J.: Caracterización estructural de vidrios del sistema SiO_2-B_2O_3-Na_2O- mediante espectroscopías IR y Raman. In: Boletín de la Sociedad Española de Cerámica y Vidrio 48.5 (2009), pp. 237–243.

[49] Tang, M.; Wang, W.; Xu, D., and Wang, Z.: Synthesis of Structure-Controlled Polyborosiloxanes and Investigation on Their Viscoelastic Response to Molecular Mass of Polydimethylsiloxane Triggered by Both Chemical and Physical Interactions. In: Industrial & Engineering Chemistry Research 55 (2016). doi: 10.1021/acs.iecr.6b03823.

[50] Tanzi, M. C.; Farè, S., and Candiani, G.: Chapter 4 - Biomaterials and Applications. In: (2019), pp. 199–287. doi: https://doi.org/10.1016/B978-0-08-101034-1.00004-9.

[51] Tavousi Tehrani, B.; Shameli-Derakhshan, S., and Jarrahi, H.: An overview on Active Confinement of Concrete column and piers Using SMAs. In: (February 2017).

[52] Thermo Fisher Scientific: Binder™ FD56 Drying Oven. 2023. url: https://www.fishersci.co.uk/shop/products/fd53-drying-oven/15692106.

[53] THERMO FISHER SCIENTIFIC: Raman and FTIR Spectroscopy. 2023. URL: https://a ssets.thermofisher.com/TFS-Assets/CAD/Application-Notes/Raman-FTIR-TechNo te-Final.pdf.

[54] UNIVERSITY OF UTAH: Rheometry Basics. 2023. URL: https://mcl.mse.utah.edu/rhe ometry-basics/.

[55] VALE, R. L.: 452. The synthesis and irradiation of polyborosilanes. In: J. Chem. Soc. (1960), pp. 2252–2257. DOI: 10.1039/JR9600002252.

[56] WANG, S.; JIANG, W.; JIANG, W.; YE, F.; MAO, Y.; XUAN, S., and GONG, X.: Multifunctional polymer composite with excellent shear stiffening performance and magnetorheological effect. In: J. Mater. Chem. C (2014). DOI: 10.1039/C4TC00903G.

[57] WANG, Y.; WANG, S.; XU, C.; XUAN, S., and JIANG, W.: Dynamic behavior of magnetically responsive shear-stiffening gel under high strain rate. In: Composites Science and Technology 127 (2016), pp. 169–176. ISSN: 0266-3538. DOI: https://doi.org/10.10 16/j.compscitech.2016.03.009.

[58] WEE SOLVE$_{GmbH}$: Oscillatory test: Frequency sweep. 2022. URL: http://www.wee-solve.de/en/frequency-sweep.html.

[59] XU, C.; WANG, Y.; WU, J.; SONG, S.; CAO, S.; XUAN, S., and JIANG, W.: Synthesis and characterization of novel SiBOC ceramics: comparison of microwave and ultrasonic application on gelation time. In: Composites Science and Technology (2017). DOI: 10 .1016/j.compscitech.2017.10.019.

[60] XU, Y.; LIAO, G., and LIU, T.: Magneto-Sensitive Smart Materials and Magnetorheological Mechanism. In: (2019). DOI: 10.5772/intechopen.84742.

[61] YANG, C.; ABANTERIBA, S., and BECKER, A.: A review of shape memory alloy based filtration devices. In: AIP Advances 10.6 (June 2020), p. 060701. DOI: 10.1063/1.5133 981.

[62] YANG, Z.; ZHOU, S.; ZU, J., and INMAN, D.: High-Performance Piezoelectric Energy Harvesters and Their Applications. In: Joule 2 (April 2018), pp. 642–697. DOI: 10.10 16/j.joule.2018.03.011.

[63] YIN, Y. and ROGERS, J. A.: Introduction: Smart Materials. In: Chemical Reviews 122.5 (2022), pp. 4885–4886. DOI: 10.1021/acs.chemrev.2c00074.

[64] ZAGHDOUDI, M., KÖMMLING, A., JAUNICH, M., WOLFF, D.: Scission, Cross-Linking, and Physical Relaxation during Thermal Degradation of Elastomers. In: (2019). DOI: 10.3390/polym11081280.

[65] ZASZCZYŃSKA, A.; GRADYS, A., and SAJKIEWICZ, P.: Progress in the Applications of Smart Piezoelectric Materials for Medical Devices. In: Polymers 12 (2020). DOI: 10.3390/polym12112754.

[66] ZHAO, J.; JIANG, N.; ZHANG, D.; HE, B., and CHEN, X.: Study on Optimization of Damping Performance and Damping Temperature Range of Silicone Rubber by Polyborosiloxane Gel. In: Polymers (2020). DOI: 10.3390/polym12051196.

[67] ZHEN, L.; PICKEN, S. J., and BESSELING, N. A. M.: Polyborosiloxanes (PBSs), Synthetic Kinetics, and Characterization. In: Macromolecules (2014). DOI: 10.1021/ma500632f.

[68] ZINCHENKO, G.; MILESHKEVICH, V. P., and KOZLOVA, N.: Investigation of the synthesis and hydrolytic degradation of polyborodimethylsiloxanes. In: Polymer Science USSR 23 (1981), pp. 1421–1429. DOI: 10.1016/0032-3950(81)90109-X.

A. Appendix

The appendix presents additional images of PBS characterization results and the data sheets of the utilized precursors. These images offer supplementary details on the morphology and chemical structure of PBS, providing a more comprehensive insight into the results presented in the fourth chapter. Furthermore, precursor data sheets are included, offering detailed information on properties and composition. This appendix serves to provide access to supplementary materials for a deeper understanding of PBS fabrication and characterization.

A.1. Additional results from characterization tests

A.1.1. Morphological Characterization

This section presents additional SEM images for PBS1 and PBS2, captured at different magnifications to offer a detailed view of their morphological characteristics. In Figure A.1 and Figure A.2, images of PBS1 reveal the presence of non-reacted boric acid on the PBS surface. Additionally, Figure A.3, Figure A.4, and Figure A.5 showcase images of PBS2, illustrating a rougher surface compared to PBS1, particularly evident at 50 and 150 magnifications.
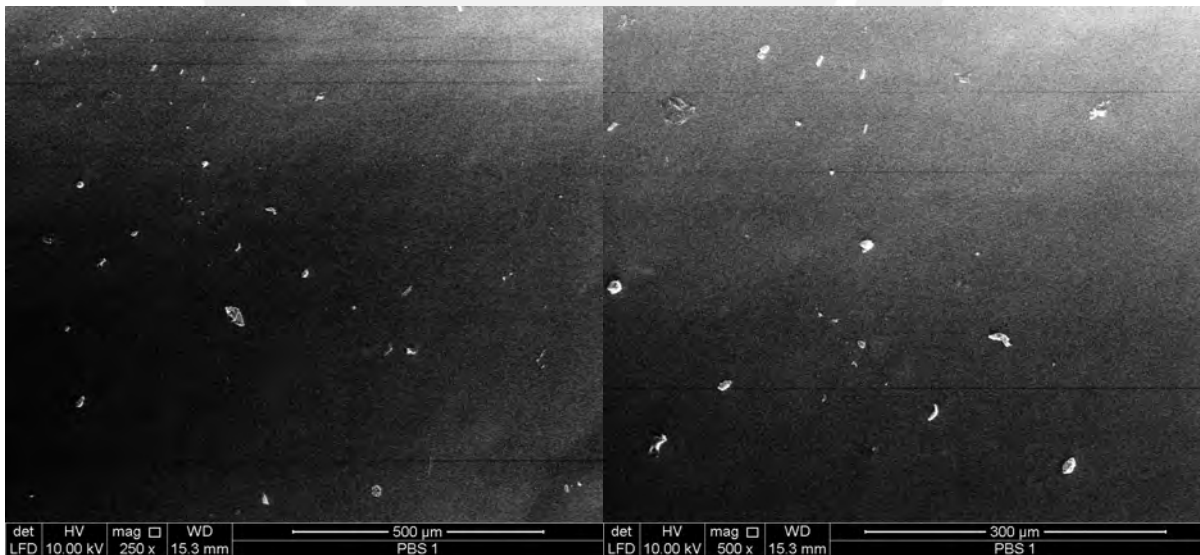
Figure A.1.: SEM images of PBS1 for 250 and 500 magnifications.
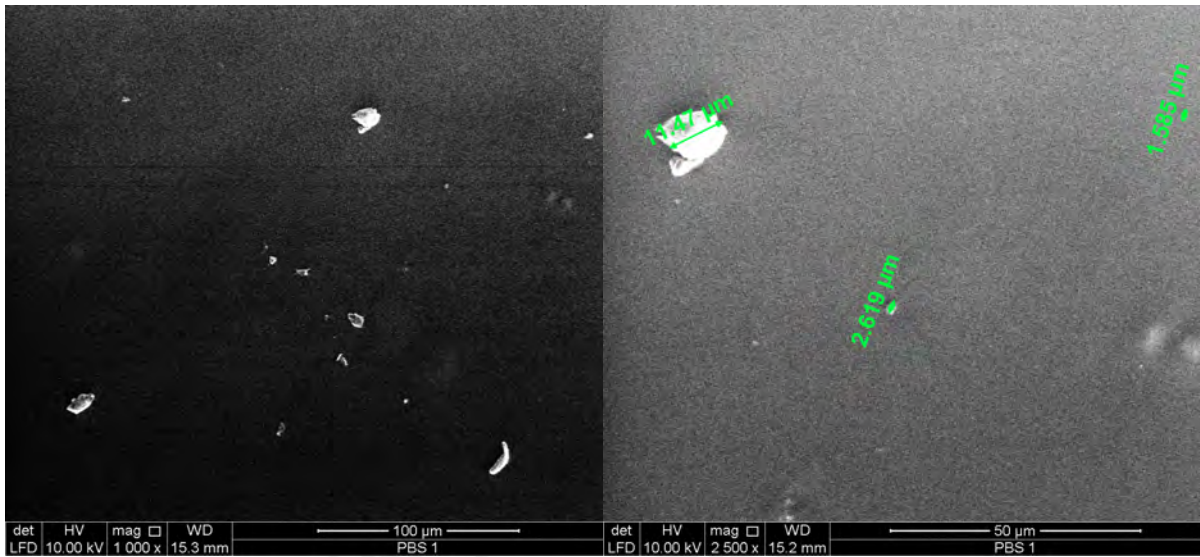
Figure A.2.: SEM images of PBS1 for 1000 and 2500 magnifications.
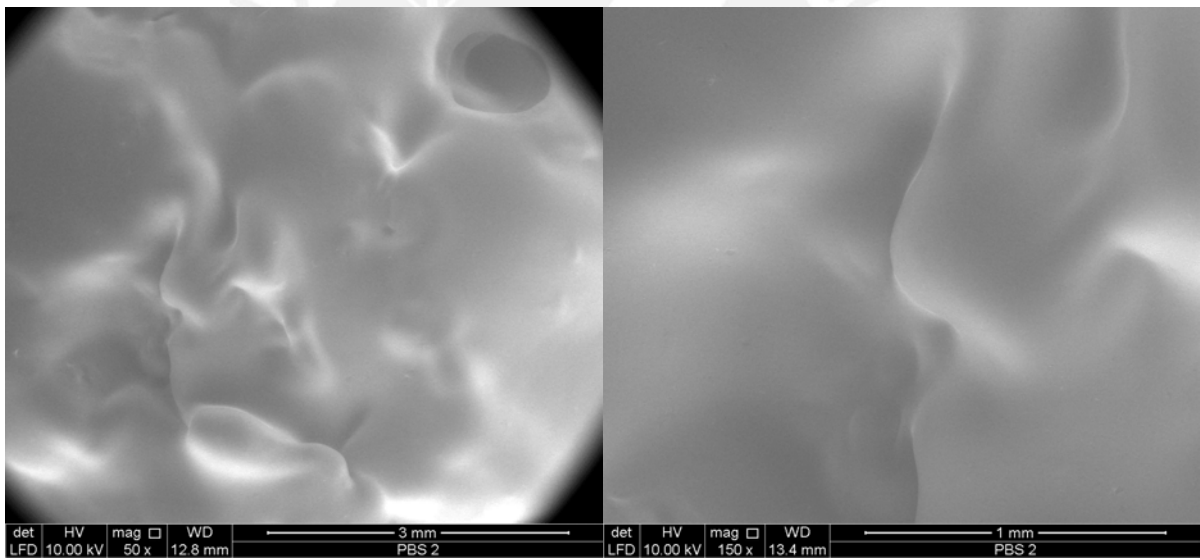

Figure A.3.: SEM images of PBS2 for 50 and 150 magnifications.
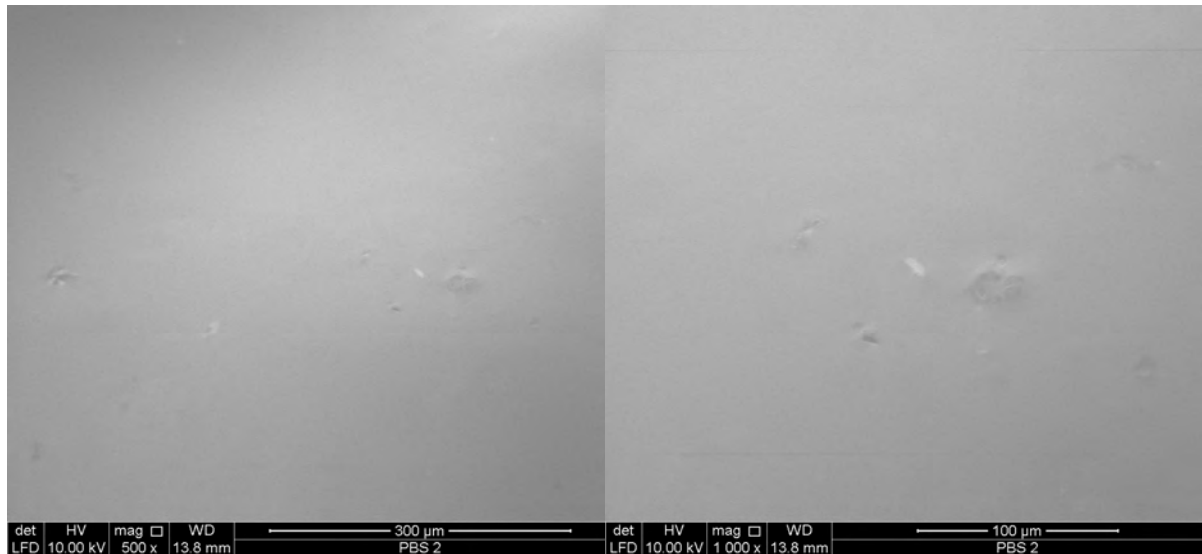
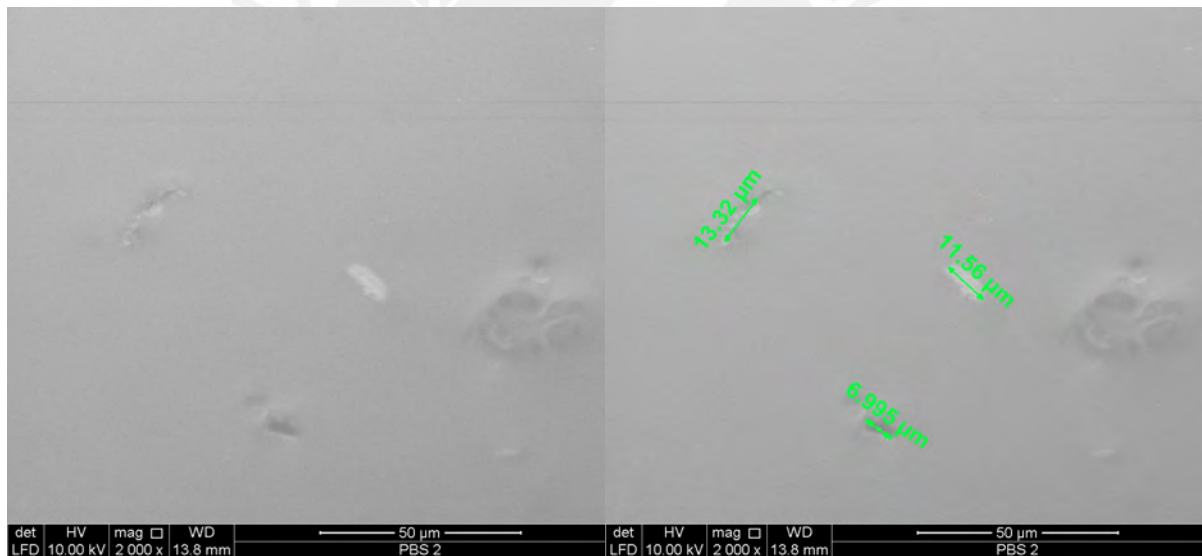Figure A.4.: SEM images of PBS2 for 500 and 1000 magnifications.

Figure A.5.: SEM images of PBS2 for 2000 magnifications.

A.1.2. Shape change test

This section presents additional graphics depicting the shape change test results for PBS1 and PBS2, showcased in Figure A.6 and Figure A.7. These graphics illustrate the average diameter measured at 10-minute intervals over a total duration of 150 minutes. Each data point on the graph includes bars indicating the maximum and minimum values, reflecting the asymmetrical deformation of PBS over time. Despite variations in the initial diameter due to sample preparation and potential human error, the graphics consistently show that both

samples exhibit the minimum shape change rate at 1 Hz. This alignment with the findings in the fifth chapter enhances the reliability of the observed trends.
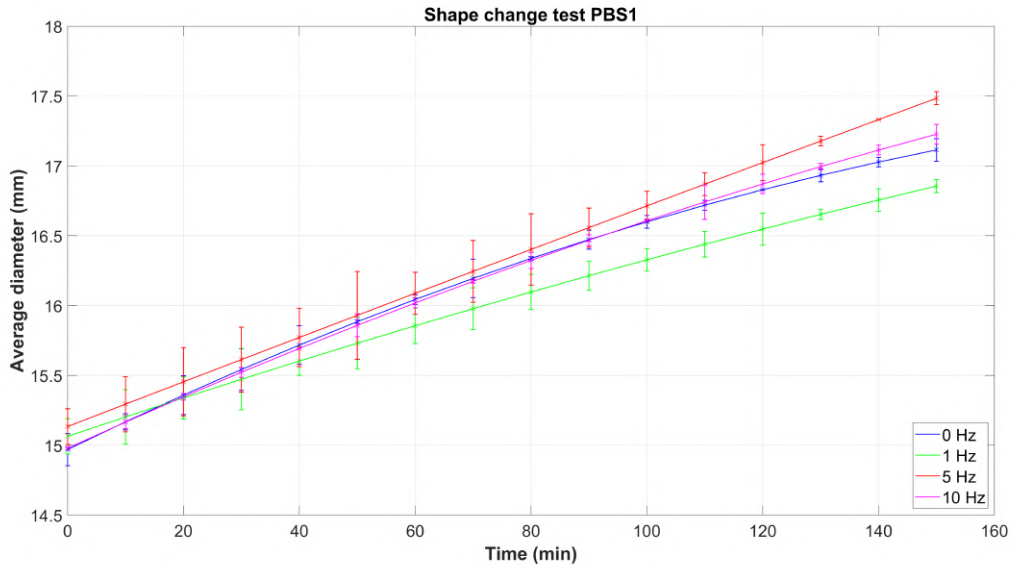

Figure A.6.: Average diameter of shape change test for PBS1
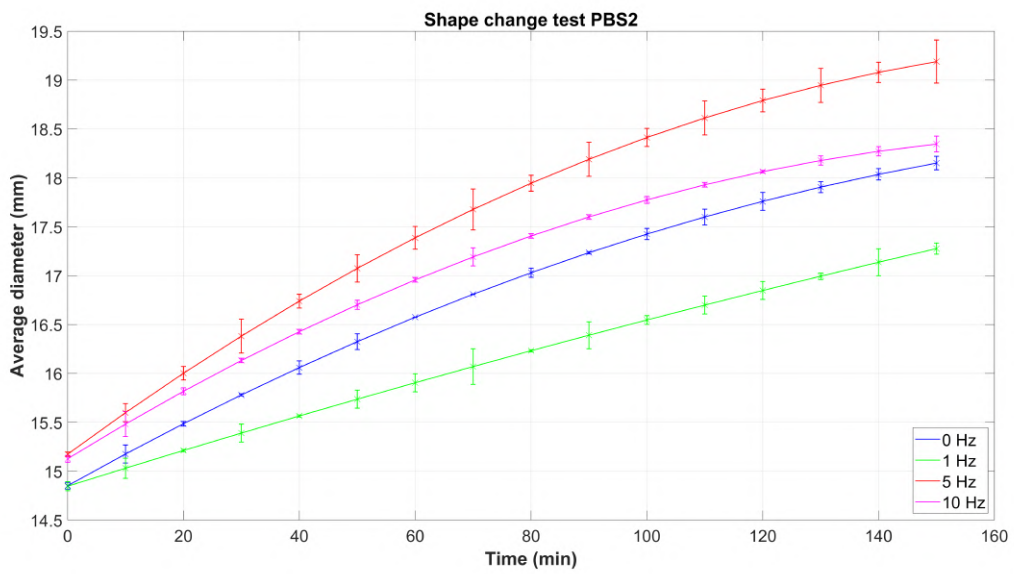

Figure A.7.: Average diameter of shape change test for PBS2

A.2. Data Sheets

In this section, you can find the data sheets containing crucial information about the composition and characteristics of PDMS and Boric Acid precursors. These sheets offer valuable details such as chemical structure, viscosity, appearance, and purity, contributing to a comprehensive understanding of the precursors used in the study.
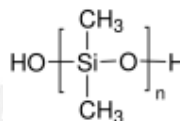
Product Specification

Product Name:
Poly(dimethylsiloxane), hydroxy terminated - viscosity ~750 cSt

Product Number: **481963**
CAS Number: 70131-67-8
MDL: MFCD01325010
Formula: C2H6OSi

TEST	Specification
Appearance (Color)	Colorless
Appearance (Form)	Liquid
Infrared spectrum	Conforms to Structure
Viscosity	650 - 900 cps
At 25 Degrees Celsius	

Specification: PRD.0.ZQ5.10000105825

Product Specification

Product Name:
Boric acid – BioReagent, for molecular biology, suitable for cell culture, suitable for plant cell culture, ≥99.5%

Product Number: **B6768**
CAS Number: 10043-35-3
MDL: MFCD00011337
Formula: H3BO3
Formula Weight: 61.83 g/mol

| TEST	Specification
Appearance (Color)	White
Appearance (Form)	Powder
Solubility (Color)	Colorless
Solubility (Turbidity)	Clear
40 mg/mL, H2O	
Iron (Fe)	$\leq$ 5 ppm
By ICP	
Magnesium (Mg)	$\leq$ 5 ppm
By ICP	
Heavy Metals (as Lead)	<= 10 ppm
DNAse, Exonuclease Detection	None Detected
RNAse Detection	None Detected
Protease by FITC-Casein	None Detected
Titration with NaOH	$\geq$ 99.5 %
UV Absorbance 260nm	$\leq$ 0.05
1M solution, H2O	
UV Absorbance 280nm	$\leq$ 0.05
1M solution, H2O	
Plant Cell Culture Test	Pass
Cell Culture Test	Pass
Endotoxin Assay	$\leq$ 1 EU/mg
Total Aerobic Count	$\leq$ 50 CFU/g
per USP	

Specification: PRD.2.ZQ5.10000006404

Selbstständigkeitserklärung

Hiermit erkläre ich, dass ich die vorliegende Arbeit selbständig und ohne Verwendung anderer als der angegebenen Hilfsmittel angefertigt habe. Die aus fremden Werken wörtlich oder sinngemäß übernommenen Gedanken sind unter Angabe der Quellen gekennzeichnet. Ich versichere, dass ich bisher keine Prüfungsarbeit mit gleichem oder ähnlichem Thema bei einer Prüfungsbehörde oder anderen Hochschule vorgelegt habe.

Ilmenau, 11.12.2023 _____

Dante Aaron Ramirez Mestanza
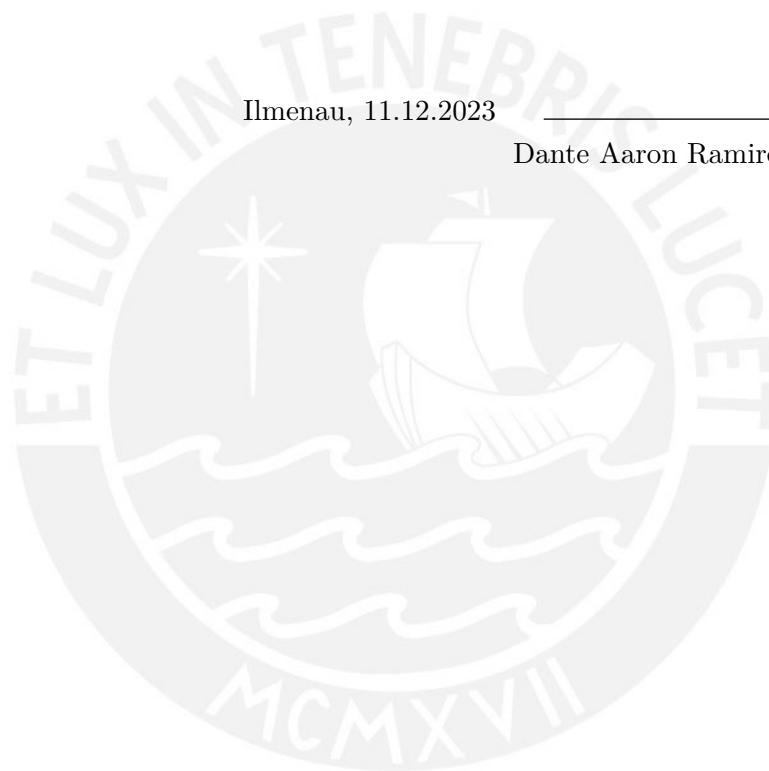
Declaration of Originality

I hereby affirm that this thesis was independently developed, and I have not utilized sources other than those explicitly cited. All direct and indirect citations are duly acknowledged. This work has not been submitted, in whole or in part, for assessment in any other context or examination. I declare that the content of this thesis is original and has not been replicated in any form elsewhere.

Ilmenau, 11.12.2023 _____

Dante Aaron Ramirez Mestanza